# Nonlinear Optics (WiSe 2018/19)

## Lecture 9: December 14, 2018

### Continue 9 Optical Parametric Amplifiers and Oscillators

9.9 Optical parametric chirped-pulse amplification (OPCPA)

9.9.1 Temporal optimization of ultrabroadband high-energy OPCPA

9.10 Passive CEP-stabilization in parametric amplifiers

9.10.1 Active versus passive CEP-locking

9.10.2 Generation of CEP-stable pulses from an OPA:

- CEP-stable IR pulses from hybrid type-II OPCPA/filamentation system
- OPCPA of a 2-μm seed pulse obtained by intrapulse DFG
- Dual-chirped infrared optical parametric amplification (DC-OPA)
- Parametric sub-cycle optical waveform synthesizers

# 9.9 Optical parametric chirped-pulse amplification (OPCPA)

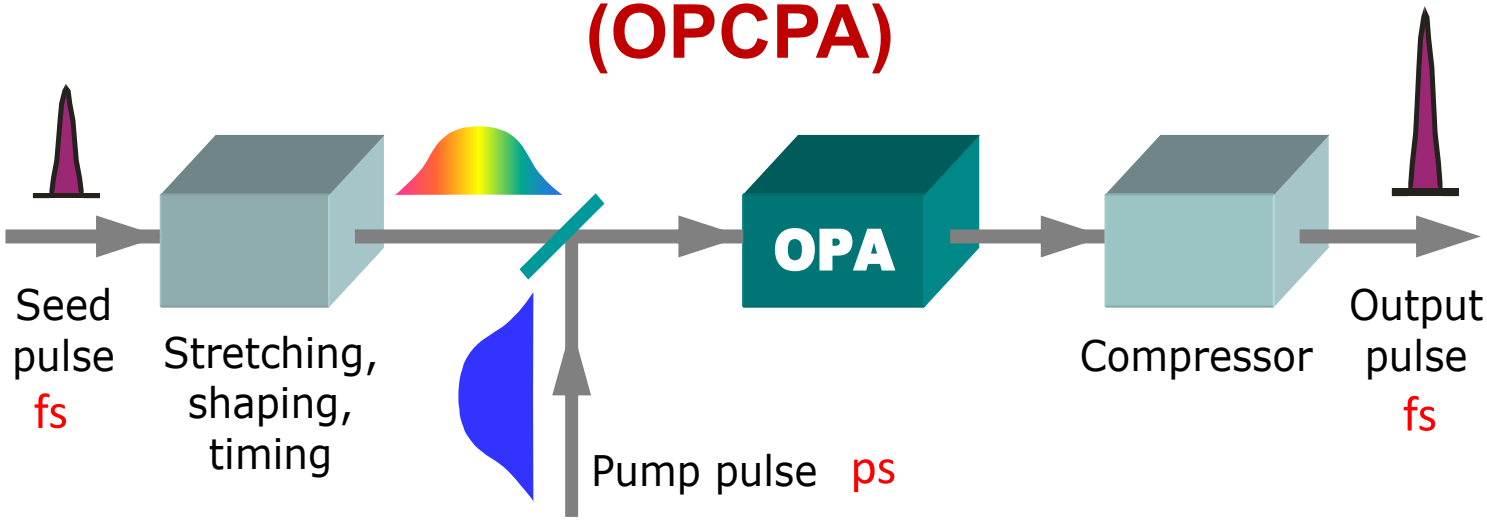


**advantages over stimulated emission based amplifier systems:**

+ gain bandwidth can be 'engineered' → **other wavelengths** (nonlinear crystal, interaction geometry)
+ large single-pass gain ($10^6$-$10^7$ in millimeters of gain crystals)
+ preserves carrier-envelope phase (CEP),
+ **passive CEP stabilization** (G. Cerullo *et al.*, Laser & Photonics Rev. **5**, 323 (2011))
+ transitions between virtual states → no energy storage → thermal loading not a problem
+ **good energy-scalability and repetition-rate scalability** ("next-generation fs sources")

- no pump-energy accumulation (high intensity pump required)
- precise pump-signal synchronization required

# 200 TW 45 fs laser based on OPCPA

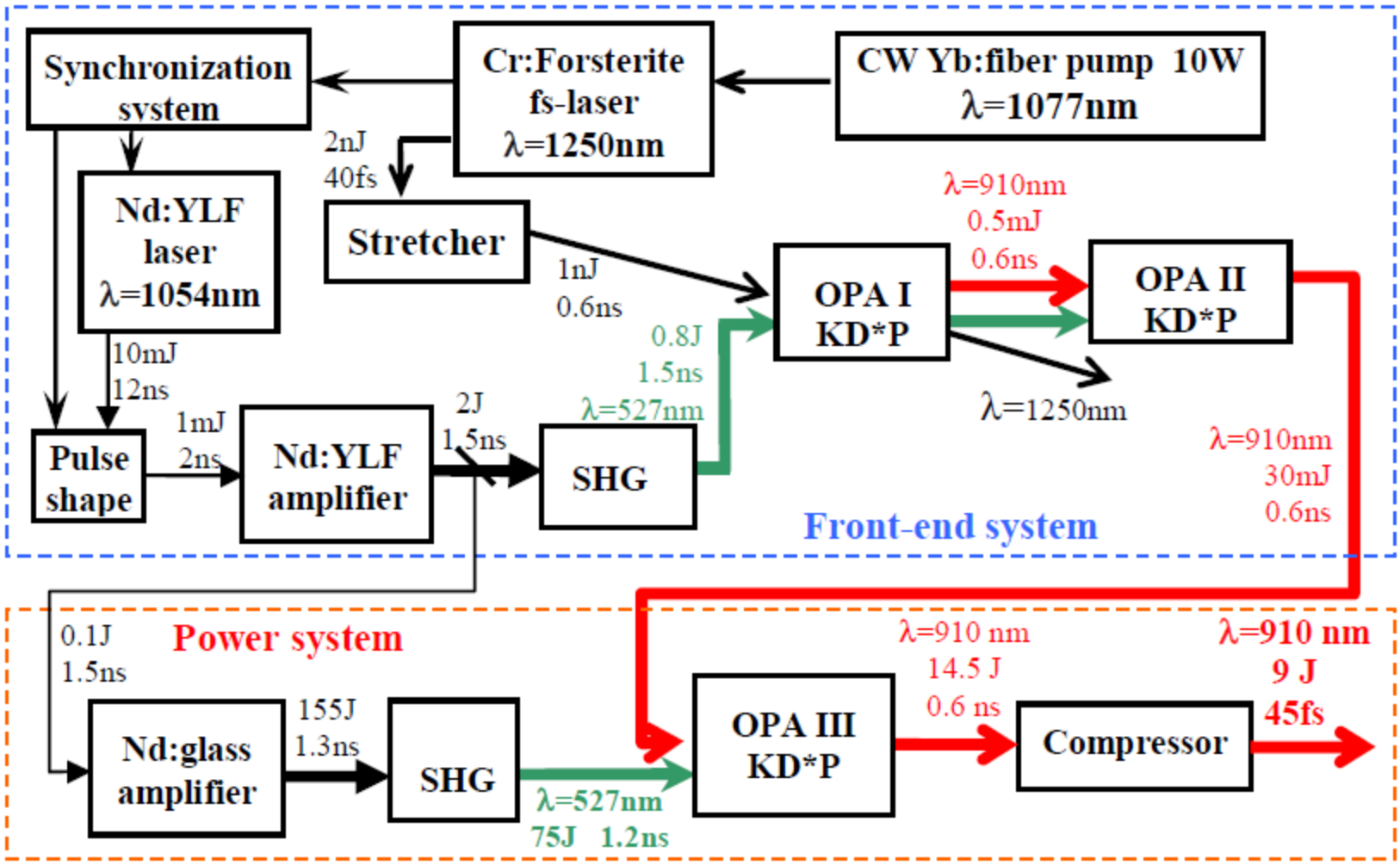


Fig. 1. Scheme of 200TW laser system based on OPAs.

V. V. Lozhkarev *et al.*, Opt. Express **14**, 446 (2006)

# 1 PW OPCPA using 100 mm LBO (SIOM, 2014)

SULF (Shanghai Superintense Ultrafast Laser Facility)

slide by Ruxin Li (SIOM)

**LBO:**
**100mm×100mm×17mm**

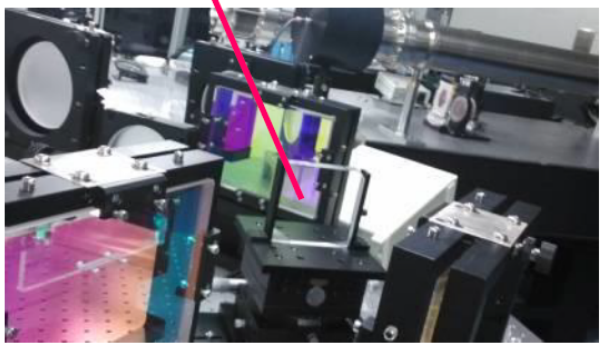

**Beam size:**
**pump: 84mm**
**signal: 82mm**

**Pulse width:**
**pump: 2.89ns**
**signal: 1.9ns**

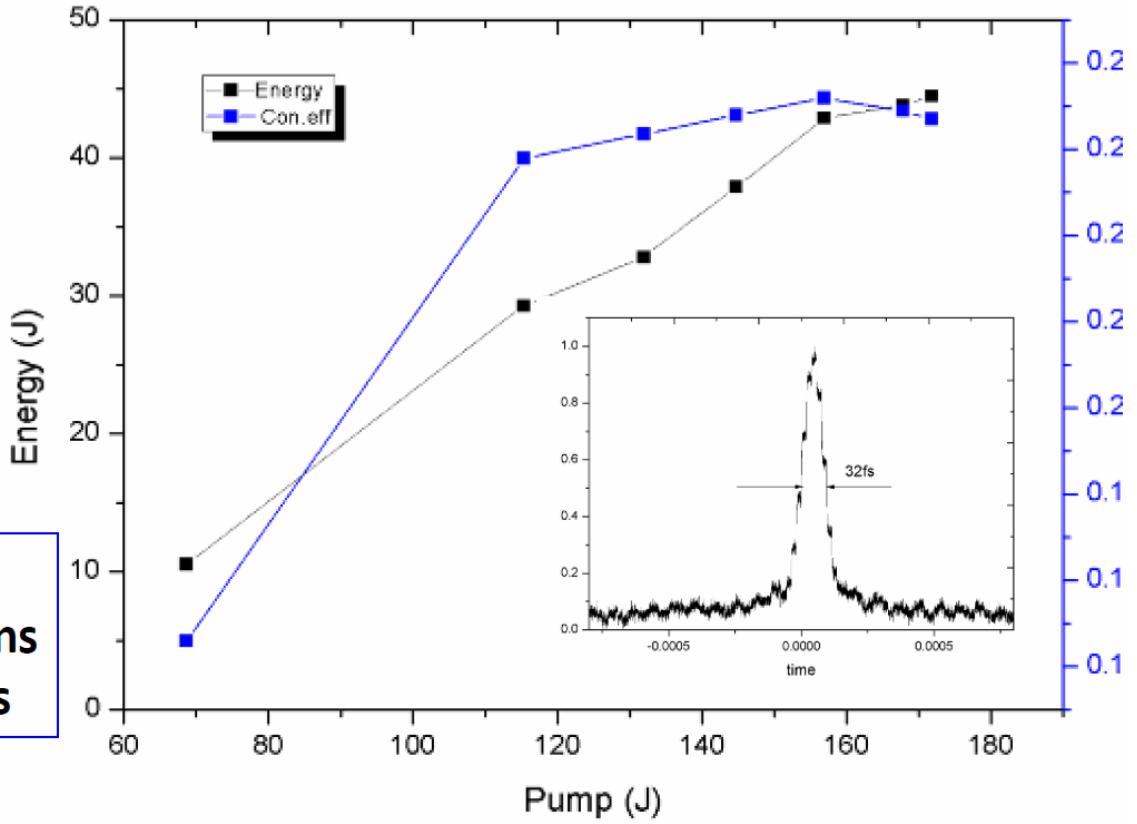


**Compressor Effi: 72%**
**Output Energy: 32.0J**
**Pulse Width: 32.0fs**
**Peak Power: 1.0PW**

**Laser Energy: 44.5J**
**Pump Energy: 167J**
**Pump fluence: 1.06GW/cm²**
**Conversion Efficiency: 26%**

SIOM 中国科学院上海光学精密机械研究所

10 PW Ti:sa CPA booster

L. Yu *et al.*, Opt. Lett. **40**, 3412 (2015)

# Next-generation high-rep-rate attoscience driver sources

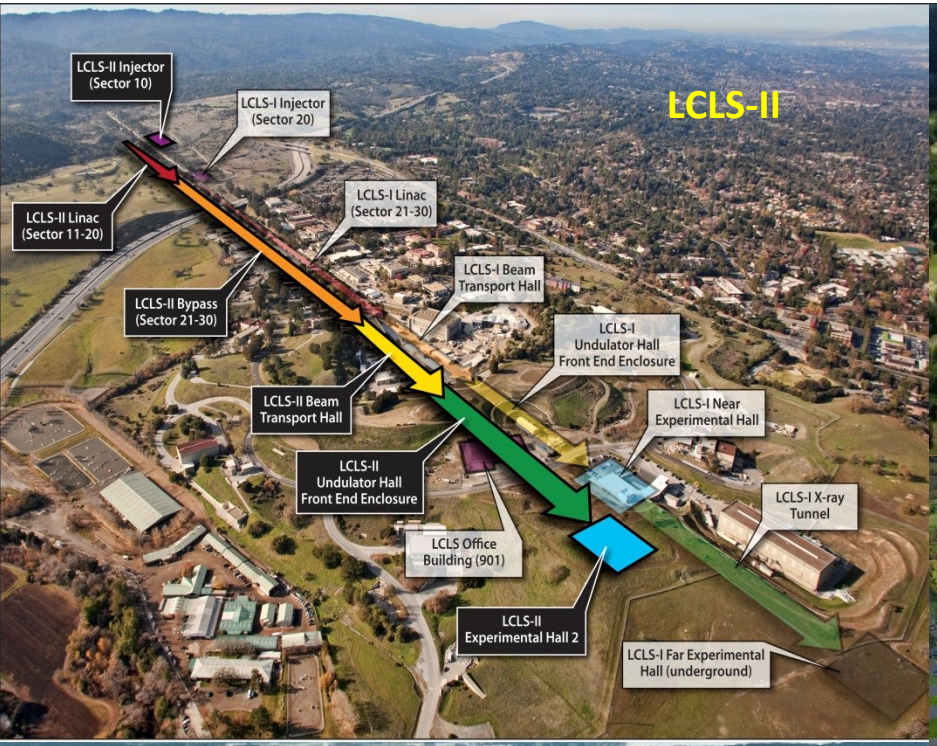

LCLS-II


SCSS


ELI-ALPS (<5fs 5mJ 100kHz)


European XFEL

FLASH

# 9.9.1 Temporal optimization of ultrabroadband high-energy OPCPA

avoid/suppress parametric superfuorescence buildup in amplification chain

simultaneous optimization of conversion efficiency, signal bandwidth, and signal-to-noise ratio (SNR)

rule of thumb: $\Delta t_s/\Delta t_p$ ranging between 0.2 to ~0.6

noise amplification leads to gain quenching

"case study" by J. Moses *et al.*, Opt. Express **17**, 5540 (2009):

spatio-temporal variation of the small-signal gain

$$g(I_p(t), \Delta k(t))$$

$$\Delta k(t) = k_p - k_s(t) - k_i(t)$$

To gauge the maximum possible conversion efficiency of the amplifier, the concept of the temporal region of significant gain of the pump pulse is useful. Consider parametric amplification of a seed pulse with spectrum centered at signal frequency $\omega_s$ by a pump pulse with center frequency $\omega_p$ such that $\omega_p = \omega_s + \omega_i$. If the idler is unseeded, prior to significant pump depletion the gain obeys the relation $G = I_s(L)/I_s(0) = 1 + (\Gamma^2/\gamma^2)\sinh^2(\gamma L)$, where $\gamma = \sqrt{\Gamma^2 - (\Delta k/2)^2}$, and $\Gamma^2 = 2\omega_s\omega_i d_{\text{eff}}^2 I_p/n_s n_i n_p \epsilon_0 c^3$. If the gain is reasonably large, i.e., $\Gamma L \gg 1$,

$$G \simeq \frac{1}{4}\exp\left(2\left[\Gamma^2 - (\Delta k/2)^2\right]^{1/2} L\right), \tag{9.49}$$

which, in the case of perfect phase matching, can be recast in the form

$$G \simeq \frac{1}{4}\exp\left(2\Gamma L\right). \tag{9.50}$$

In this case, since $\Gamma \sim \sqrt{I_p}$, the gain is time-dependent and follows the pump pulse intensity profile: $G(t) \sim \exp[\sqrt{I_p(t)}]$. $G(t)$ is plotted in Fig. 9.26(a) alongside $I_p(t)$ for a Gaussian pump pulse and unchirped, phase-matched seed. The peak gain is 100 and the plotted gain profile is normalized to 1. Significant gain will only be possible for a seed pulse overlapped with the pump pulse within a central region around $t = 0$. The shaded interval of Fig. 9.26(a) corresponds to the region $t < |t_g|$ where $G(t) \geq e^{-1}G_0$, with peak gain $G_0 = G(t = 0)$.

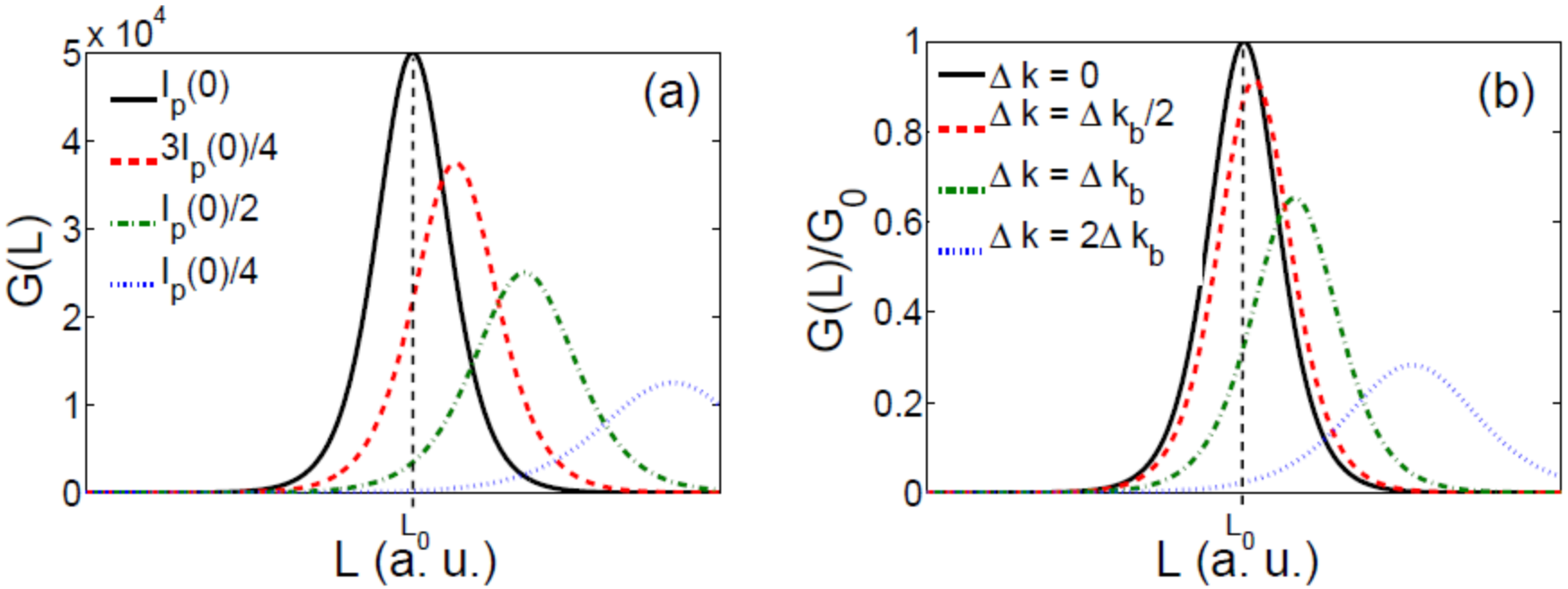


Figure 9.25: Signal gain, $G$, versus propagation length, $L$, for a phase-matched ($\Delta k = 0$) parametric amplifier that has a peak gain $G_0 = 5 \times 10^4$, calculated by solution of the coupled nonlinear wave equations describing parametric amplification for monochromatic plane waves. $L_0$ is the length at which the gain curve peaks with an initial pump intensity $I_p(0)$, i.e., the length at which the pump is fully depleted and before backconversion occurs. In (a), gain curves corresponding to lower pump intensity are also shown (representing, for example, the amplification that occurs along the wings of a pump pulse relative to its peak). In (b), the effect of increasing $\Delta k$ is shown, with an initial pump intensity $I_p(0)$ for all curves. $\Delta k_b$ is the wavevector mismatch that reduces the gain at $L_0$ by $1/e$. [15]

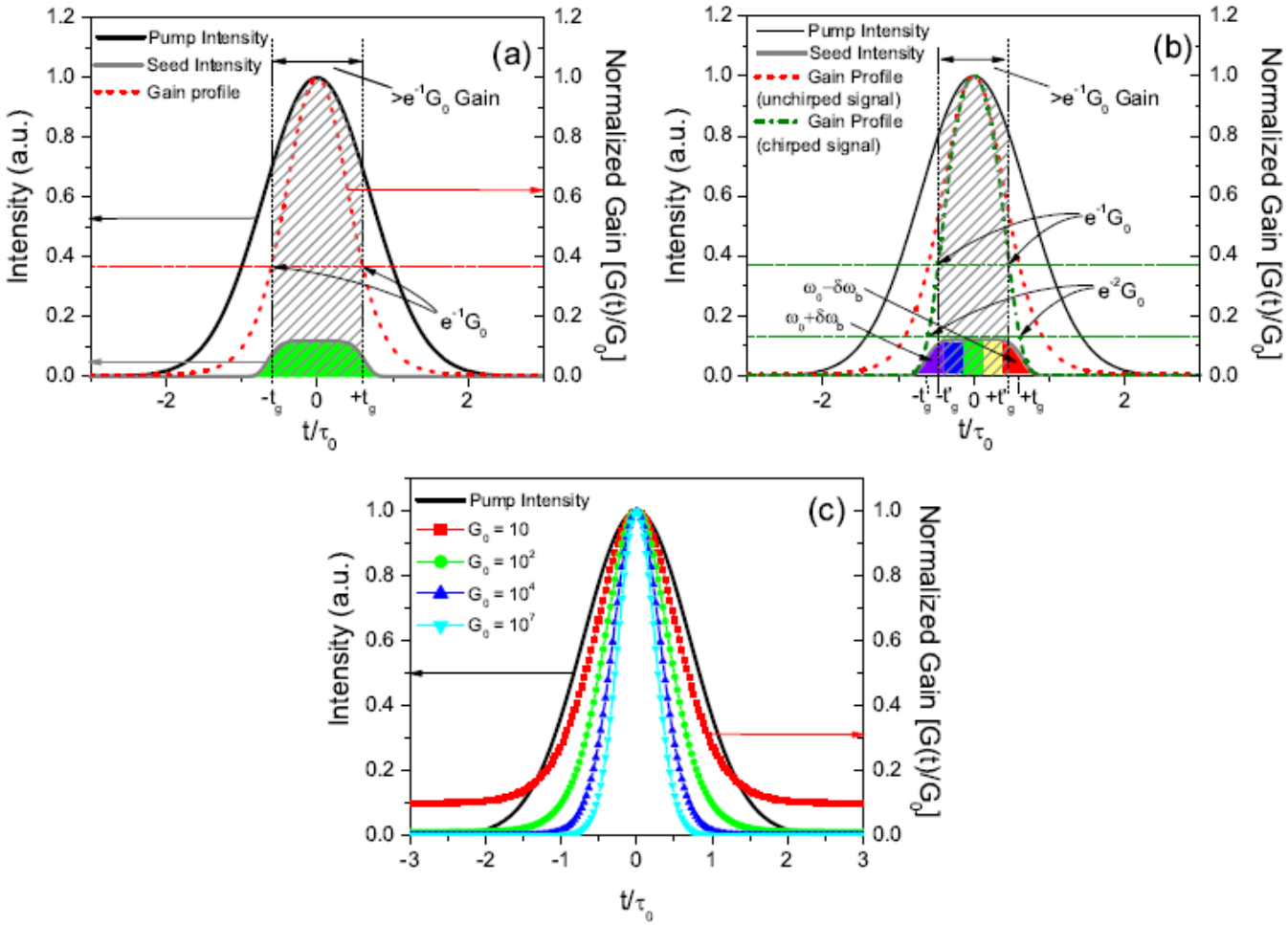


Figure 9.26: (a) Normalized Gaussian pump pulse profile (black, solid) and corresponding temporal gain profile (red, dashed) of an unchirped phase-matched parametric amplifier with a peak gain $G_0 = 100$. The shaded region indicates the region of the pump pulse where gain is $\geq \mathrm{e}^{-1}G_0$. A suitable seed pulse is also indicated. (b) The equivalent of (a) but assuming a seed spectrum extending from $\omega_s - \delta\omega_b$ to $\omega_s + \delta\omega_b$ and chirped such that frequencies $\omega_s \pm \delta\omega_b$ just fit within the region of significant gain corresponding to (a). (c) Normalized pump intensity profile and corresponding gain profiles for various values of the peak gain for an unchirped phase-matched amplifier. [15]

Let us calculate the centroid bounds, $\pm t_g$, corresponding to a gain $G(t_g) = e^{-1}G_0$, in the case of perfect phase matching. If we define the small-signal gain $g(t) = 2\Gamma(t)L$ and $g_0 = g(0)$, we obtain

$$\frac{g(t_g)}{g_0} = \sqrt{\frac{I_p(t_g)}{I_p(0)}} = \frac{g_0 - 1}{g_0}. \tag{9.51}$$

For a Gaussian pump pulse, described by $I_p(t) = I_0 \cdot \exp(-(t/\tau_0)^2)$ with FWHM duration $\Delta t_p = 2\tau_0 \cdot \sqrt{\ln 2}$, we may rearrange Eq. (9.51) to find

$$t_g = \frac{\Delta t_p}{2\sqrt{\ln 2}} \sqrt{-2\ln\left[1 - 1/\ln(4G_0)\right]}. \tag{9.52}$$

Since pump depletion will typically occur only where there is significant signal gain, $t_g$ thus gives a measure of the maximum possible energy extraction from the pump. Note that $t_g$ is a function of the peak gain $G_0$, and that a power amplification stage with low $G_0$ will have a larger gain centroid width than a pre-amplification stage with high $G_0$. Thus, the power amplier can extract more energy from the pump pulse, resulting in a higher maximum conversion efficiency. Figure 9.26(c) plots the temporal gain profile of an amplifier with unchirped signal pulse for several values of $G_0$, each curve normalized to 1, and Table 9.1 tabulates the pump centroid width. The difference in $t_g$ for pre- and power amplifiers implies that a different seed pulse chirp will optimize amplification at each stage. For example, a power amplifier stage with $G_0 = 10^2$ has 1.5× wider a region of significant gain than a preamplifier stage with $G_0 = 10^5$.

Table 9.1: Width of temporal region of significant gain versus peak gain

| $G_0$ | 10 | $10^2$ | $10^3$ | $10^4$ | $10^5$ | $10^6$ | $10^7$ |
|---|---|---|---|---|---|---|---|
| $2t_g/\Delta t_p$ | 0.955 | 0.725 | 0.609 | 0.534 | 0.483 | 0.443 | 0.412 |
| $2t'_g/\Delta t_p$ | 0.726 | 0.571 | 0.483 | 0.425 | 0.385 | 0.353 | 0.335 |

For an OPCPA, we need to include also the temporally-varying wavevector mismatch, $\Delta k(t)$. According to Eq. (9.49), wavevector mismatch leads to a reduction in the gain at the wings of the signal pulse if phase-matched at the center of the pulse. In Fig. 9.26(b), the red (dashed) curve represents the gain profile of the unchirped signal pulse of Fig. 9.26(a), while the green (dot-dashed) curve includes the effects of the temporally-varying wavevector mismatch and the resulting decrease in the small-signal gain. The signal pulse is linearly chirped such that the edges of the phase-matching bandwidth, $\omega - \omega_s = \pm\delta\omega_b$, where $G(\omega_s \pm \delta\omega_b) = e^{-1}G(\omega_s)$, are mapped to coordinates $t = \pm t_g$. The new temporal region of significant gain, $-t'_g < t < t'_g$, where $G(t'_g) = e^{-1}G_0$, is narrower.

In principle, as the signal chirp is increased, the region $-t_g < t < t_g$ will on average contain signal frequencies that are closer to the phase-matched frequency; $\Delta k$ remains small across the bounds and $t'_g$ tends to $t_g$, increasing the maximum possible conversion efficiency. However, the larger the chirp, the smaller the portion of the signal bandwidth that will fit within the region $-t'_g < t < t'_g$, and thus the smaller the effective amplifier bandwidth. In the other limiting case of vanishingly small chirp, all the seed colors see approximately the peak pump intensity; in this case, $t'_g$ is determined solely by phase matching, and $t'_g \ll t_g$. The bandwidth approaches the full phase-matching bandwidth, but the energy extraction is limited since only a small temporal window of the pump can be depleted.

# trade-off between conversion efficiency and bandwidth

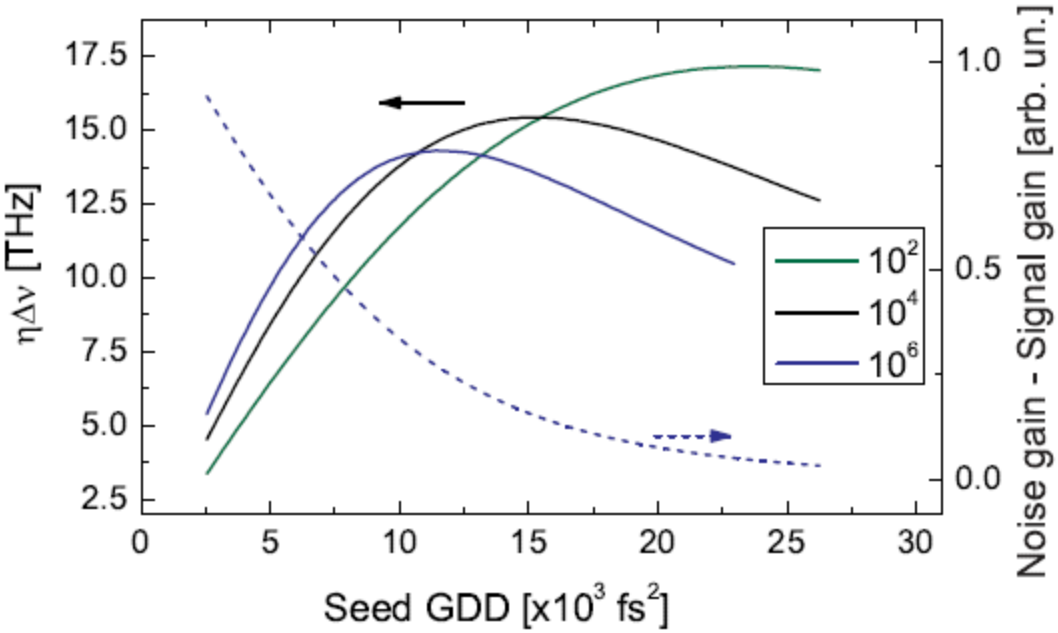


$\omega_s = \omega_i = \omega_p/2$

Figure 9.27: (solid lines) Efficiency-bandwidth products, $\eta\Delta\nu$, obtainable from the OPCPA for different values of the seed chirp (GDD) and peak gains of $10^2$, $10^4$ and $10^6$. (dashed curve) Total noise gain subtracted by total signal gain for $G_0 = 10^6$. Curves are calculated for 1.047-$\mu$m pump and 2.094-$\mu$m signal and idler mixing in 3 mm of PPSLT. The pump is 9-ps long. [15]

chirping seed influences $\Delta k(t)$

**optimum chirp depends on $G_0$ (different in each stage!)**

analysis of Eq. (9.49). Figure 9.27 plots the efficiency-bandwidth product calculated from Eq. (9.49) for given values of the peak gain $G_0$, varying the seed chirp and thus influencing the corresponding mismatch function $\Delta k(t)$. For later comparison, we consider the amplifier materials and geometry that will be discussed in section 3, and operate at degeneracy (i.e., $\omega_s = \omega_i = \omega_p/2$). We approximate the wave-vector mismatch for the broadband amplifier to second-order (with first-order term vanishing due to the matched signal and idler group velocities) by $\Delta k(\omega) = -(\omega - \omega_s)^2 \beta_2(\omega_s)$, where $\beta_2(\omega_s) = \partial^2 k/\partial\omega^2|_{\omega_s}$ is the material group-velocity dispersion (GVD) evaluated at central signal frequency $\omega_s$. The chirp is linear and each component $\omega$ is mapped at $t = (\omega - \omega_s)/\text{GDD}$ (with group-delay dispersion, GDD). Since significant energy extraction from the pump occurs only where there is significant signal gain, *efficiency* was calculated as the fraction of pump energy included in the bounds $-t_g' < t < t_g'$, and the *bandwidth* corresponds to $2\delta\omega_g/2\pi$, where we define $\omega_s \pm \delta\omega_g$ as the frequencies mapped to $t = \pm t_g'$. Figure 9.27 demonstrates a clear optimum chirp for each value of $G_0$, as expected, since efficiency increases and bandwidth decreases with increasing chirp. In order to compare the gain width of the unchirped, phase-matched amplifier to that of the chirped-pulse amplifier optimized for maximum efficiency-bandwidth product, the values of $t_g'$ corresponding to the optimum chirp at each $G_0$ are tabulated in the second line of Table 1. The parameters $2t_g/\Delta t_p$ and $2t_g'/\Delta t_p$ exhibit the same behavior as $G_0$ is varied: larger peak gains result in narrower regions of significant gain. Consistently, $t_g' < t_g$.

# SNR degradation due to superfluorescence buildup

amplifier seeded by both signal and quantum noise

signal gain $\neq$ noise gain

initial quantum noise is stationary, i.e., seed fluctuations of all frequencies are present at all times

$\rightarrow$ phase-matched quantum noise is available at all times

noise gain profile is like the signal gain profile of an unchirped, phase-matched amplifier, with $\Delta k = 0$, at all times

**local gain of signal and noise photons are different**

noise temporal gain profile is determined solely by local pump intensity, while signal temporal gain profile is determined by both local pump intensity and $\Delta k(t)$

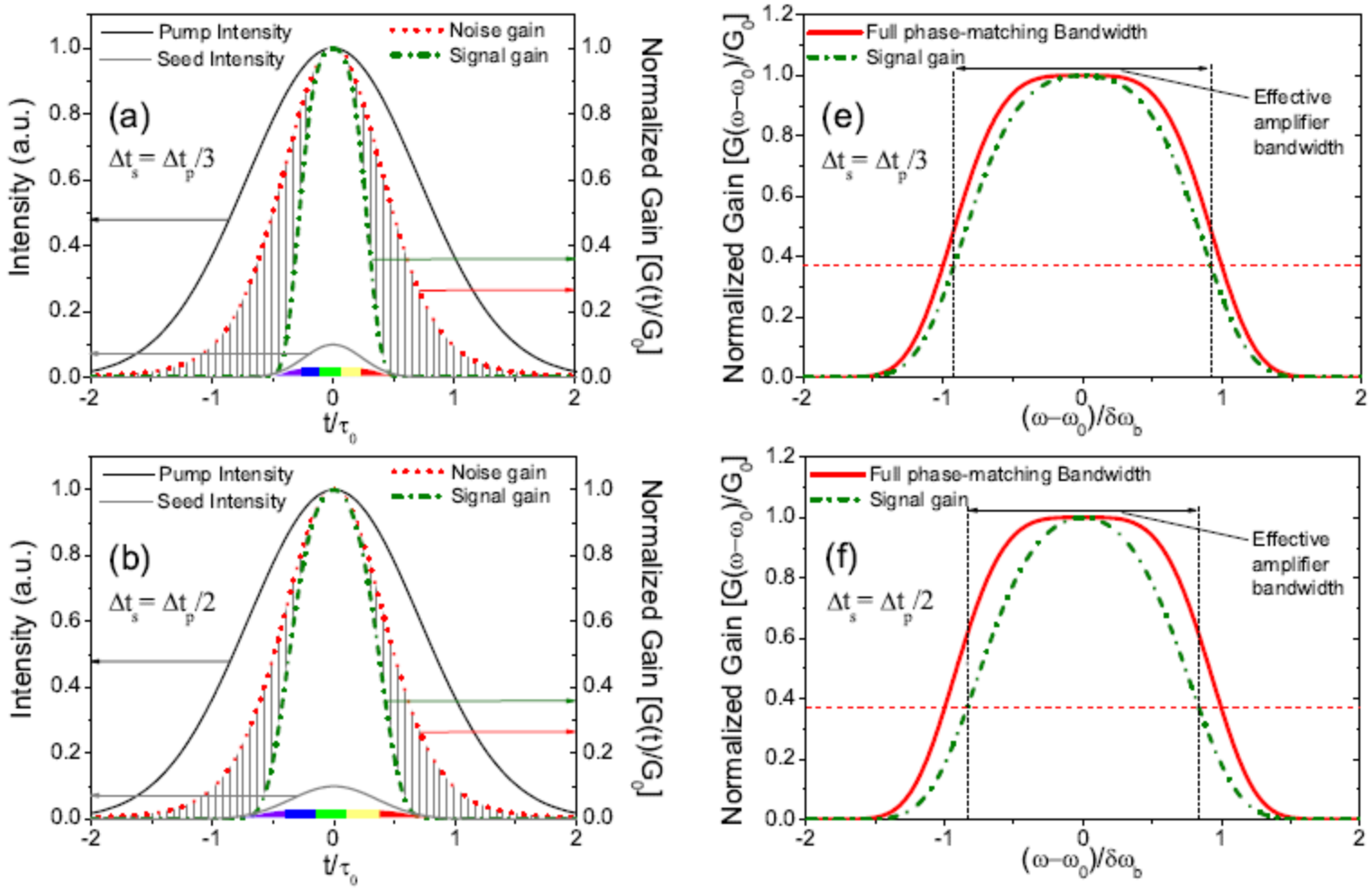


Figure 9.28: (a-d) Gaussian pump (black, solid) and seed (gray, solid) intensity profiles with corresponding signal gain (green, dot-dashed) and noise gain (red, dotted) profiles for several ratios of seed and pump pulse durations ($\Delta t_s/\Delta t_p$). The shaded region represents the difference between noise and signal gain. The chirp of the signal pulse is represented by colored bars. (e-h) Corresponding signal gain profiles (green, dot-dashed) in the frequency domain, plotted alongside the full phase-matching bandwidth of the amplifier (red, solid). [15]

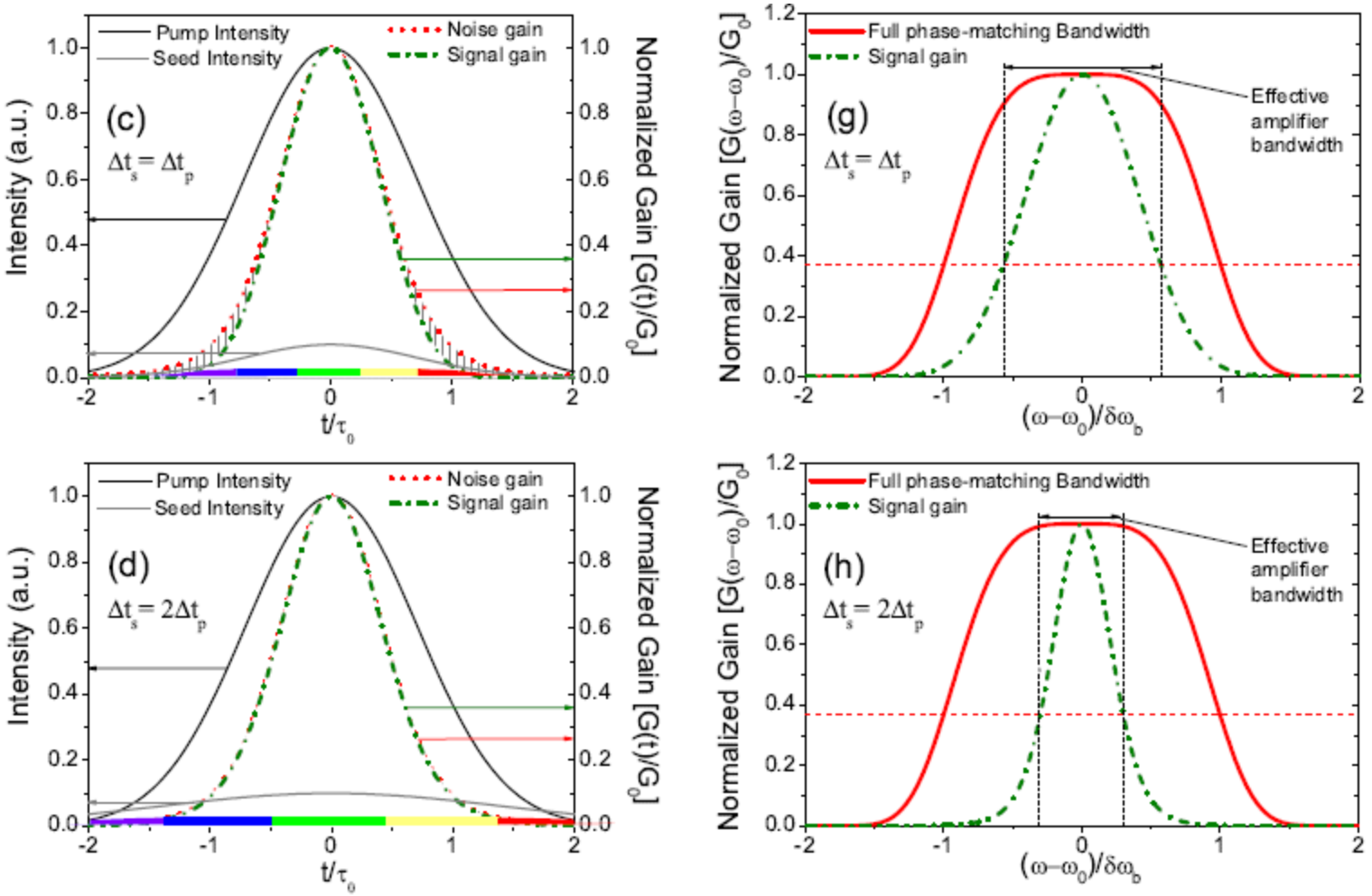


Figure 9.28: (a-d) Gaussian pump (black, solid) and seed (gray, solid) intensity profiles with corresponding signal gain (green, dot-dashed) and noise gain (red, dotted) profiles for several ratios of seed and pump pulse durations ($\Delta t_s/\Delta t_p$). The shaded region represents the difference between noise and signal gain. The chirp of the signal pulse is represented by colored bars. (e-h) Corresponding signal gain profiles (green, dot-dashed) in the frequency domain, plotted alongside the full phase-matching bandwidth of the amplifier (red, solid). [15]

J. Moses *et al.*, Opt. Express **17**, 5540 (2009)  (details in manuscript)

modelling of  2.1-μm OPCPA in

J. Moses *et al.*, Opt. Lett. **34**, 1639 (2009)  (discussed later!)

amplifier is pumped by a 9-ps FWHM Gaussian pulse at 1.047 $\mu$m and seeded by a broadband pulse at 2.094 $\mu$m, for operation around degeneracy. The interaction was calculated in a 3-mm long periodically-poled stoichiometric lithium tantalate (PPSLT) crystal. The seed had a super-Gaussian spectrum ($I_s(\omega) \sim \exp[-(\omega - \omega_s)^8]$) with FWHM bandwidth of 69 THz, which well matches the 15-fs (~2-optical-cycle) phase-matching bandwidth of the amplifier. These input parameters are close to the experimental conditions of Ref.

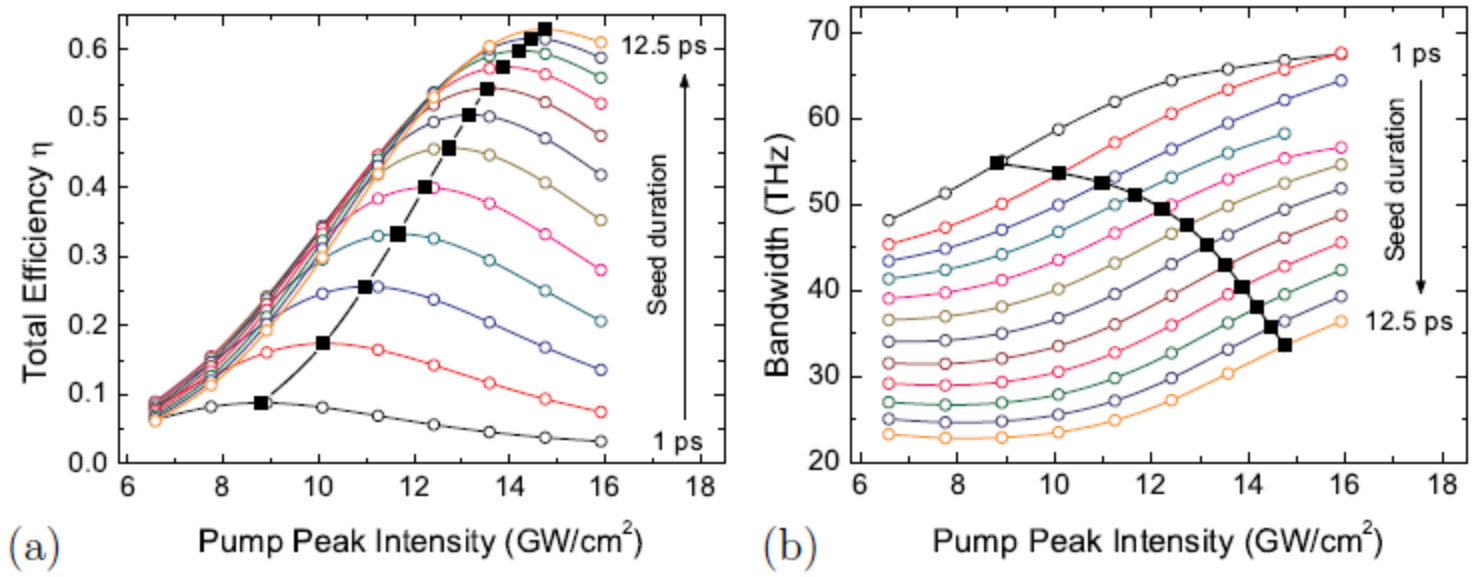


Figure 9.29: Efficiency (a) and bandwidth (b) of the OPCPA process for various seed durations and pump peak intensities, for the case $E_p/E_s = 10^4$. Squares of panel (a) highlight the highest efficiency, $\eta_{max}$, obtainable for a given seed duration; the corresponding bandwidths, $\Delta\nu$, are indicated as filled squares in panel (b). [15]

(i) amplified bandwidth decreases with increasing seed pulse duration, due to the progressively lower gain experienced by the wings of the spectrum

(ii) for each seed pulse duration there is an optimum peak intensity that guarantees the highest efficiency [squares in (a)] (higher intensities induce back-conversion at the peak of the pump pulse that exceeds additional conversion at the wings)

(iii) as seed duration is increased, the maximum possible conversion efficiency increases

(iv) for a given seed duration, as the amplifier reaches maximum conversion the bandwidth increases with intensity due to saturation of gain at the center of the pulse and preferential amplification at the wings.

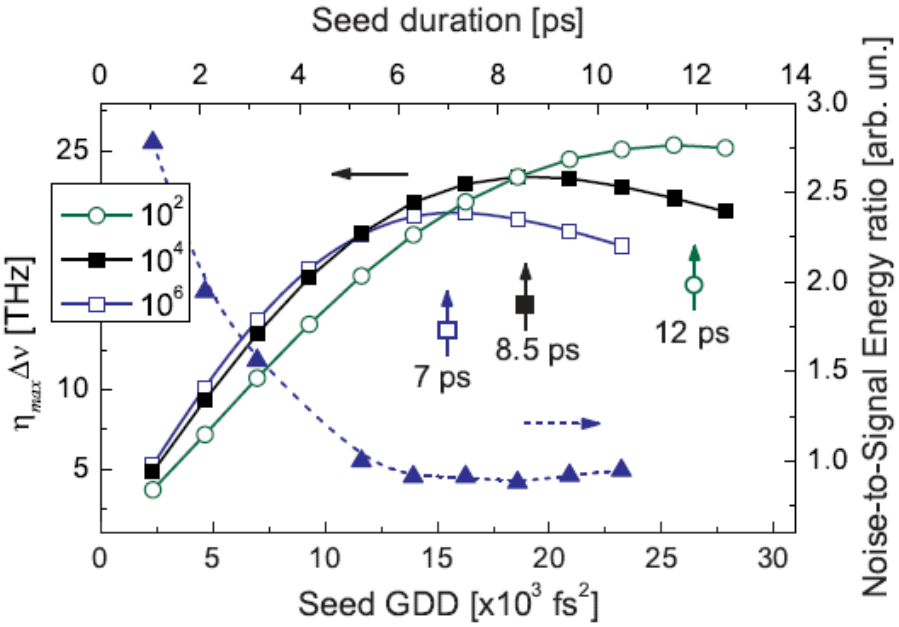


Figure 9.30: Best gain-bandwidth products obtainable from the OPCPA for various seed durations and pump-to-signal energy ratios of $E_p/E_s = 10^2$ (circles), $E_p/E_s = 10^4$ (filled squares) and $E_p/E_s = 10^6$ (open squares). The seed durations corresponding to the best performances at the three operating regimes are shown. The increase in noise relative to signal during amplification is shown for the data points of the $E_p/E_s = 10^6$ curve (triangles). [15]

$$(\Delta t_s/\Delta t_p)_{opt} \approx a\sqrt{-2\ln\left[1 - 1/\ln(2E_p/E_s)\right]}, \tag{9.55}$$

where $a = 2.1$, and therefore $(\Delta t_s)_{opt} \simeq 1.7(2t_g)$. The extra factor of 1.7 can be attributed to the increase in temporal gain profile width due to amplifier saturation: gain at the peak of the pump pulse saturates before gain at the wings does, which pushes out the wings of the gain profile. Even with the effects of saturation, however, the simple non-pump-depletion-regime analysis in the previous section still recovers the scaling of $(\Delta t_s/\Delta t_p)_{opt}$ with $E_p/E_s$.

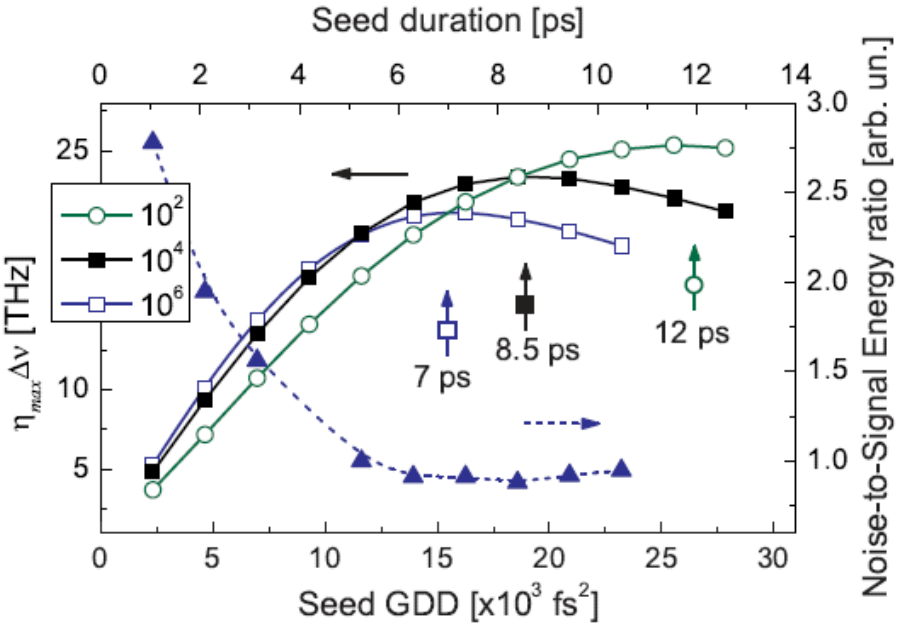


Figure 9.30: Best gain-bandwidth products obtainable from the OPCPA for various seed durations and pump-to-signal energy ratios of $E_p/E_s = 10^2$ (circles), $E_p/E_s = 10^4$ (filled squares) and $E_p/E_s = 10^6$ (open squares). The seed durations corresponding to the best performances at the three operating regimes are shown. The increase in noise relative to signal during amplification is shown for the data points of the $E_p/E_s = 10^6$ curve (triangles). [15]

Figure 9.30 plots the calculated degradation of SNR as a function of seed chirp (triangles). As predicted, the SNR performance improves significantly as the seed chirp increases, leveling off at close to the same value that maximizes the efficiency-bandwidth product. This completes the confirmation of a general conclusion of the previous section regarding OPCPA optimization: a small sacrifice in amplifier bandwidth relative to the full phase-matching bandwidth of the amplifier simultaneously allows optimal efficiency-bandwidth product and good robustness of SNR.

**numerical result** **experiment**

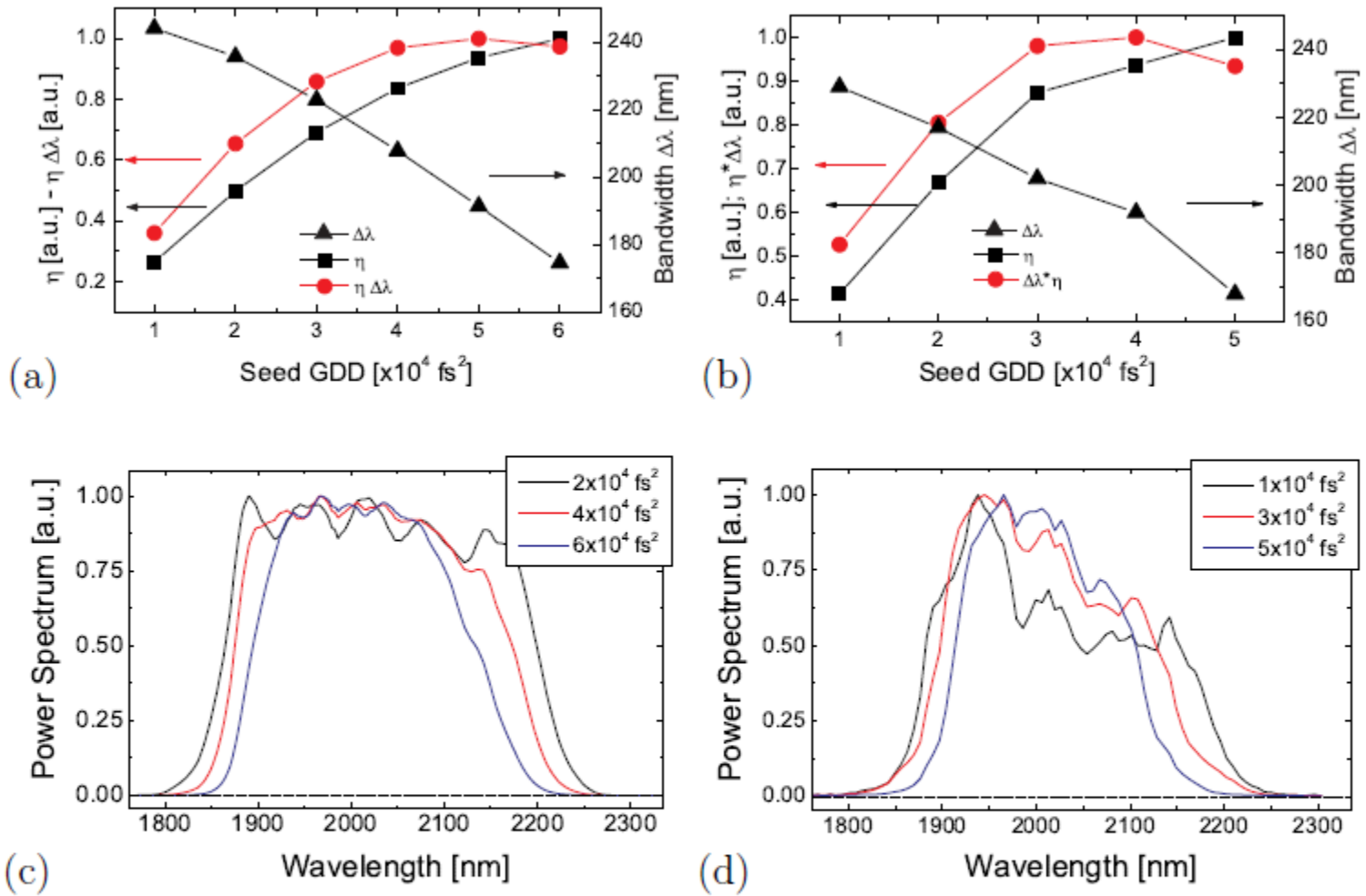


Figure 9.32: Comparison between numerical simulations [(a),(c)] and experiments [(b),(d)] for a 3-mm long, 9-ps pumped, PPSLT-based amplifier. (a)-(b) Best efficiencies and bandwidths as a function of seed chirps. (c)-(d) Amplified spectra corresponding to the maximum efficiencies for the three given seed chirps. [15]

# Conclusions:

1. simultaneous amplification of signal and background superfluorescence can be treated as simultaneous chirped-pulse and non-chirped-pulse amplification, respectively. Instantaneous signal amplification is sensitive both to the local pump intensity and instantaneous wavevector mismatch, whereas the instantaneous noise amplification is sensitive to only the local pump intensity.

2. crucially important parameter: $\Delta t_s/\Delta t_p$ as seed chirp increases, the maximum conversion efficiency increases, the amplifier bandwidth decreases, and the SNR increases. A small sacrifice in effective amplifier bandwidth relative to the full phase-matching bandwidth of the amplifier can significantly improve the SNR

3. optimal optimum $\Delta t_s/\Delta t_p$ depends on gain.

# Practical consequences for OPCPA design:

high-gain parametric amplifier is often split into two or more stages:
pre-amplification: high gain
power ('booster') amplification: relatively low gain
as peak gain decreases, both maximum achievable conversion efficiency and maximum achievable efficiency-bandwidth product increase. Therefore, by placing most of the gain in a pre-amplifier stage, and only $10^2$ gain or lower in the final stage, the final peak power of the amplifier can be maximized.

optimize the signal chirp in each stage!!!

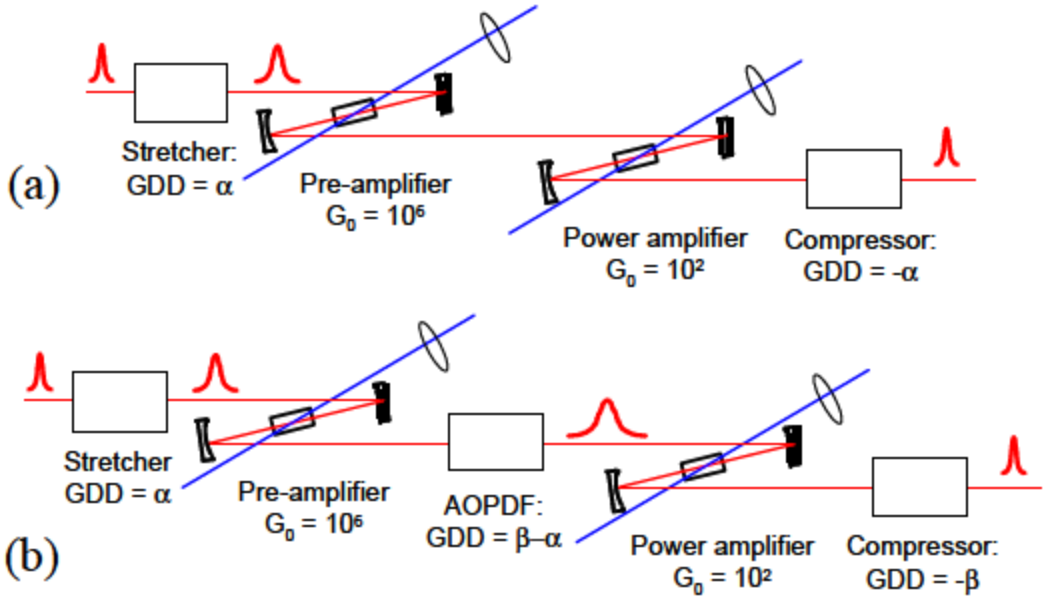


Figure 9.33: Schematics of two-stage OPCPA system designs. In (a), the signal chirp in pre- and power amplifiers must be the same. In (b), a third dispersive element allows independent optimization of $\Delta t_s/\Delta t_p$ at each stage. [15]

# 9.10 Passive CEP-stabilization in parametric amplifiers

## 9.10.1 Active versus passive CEP-locking

## Active carrier-envelope phase locking

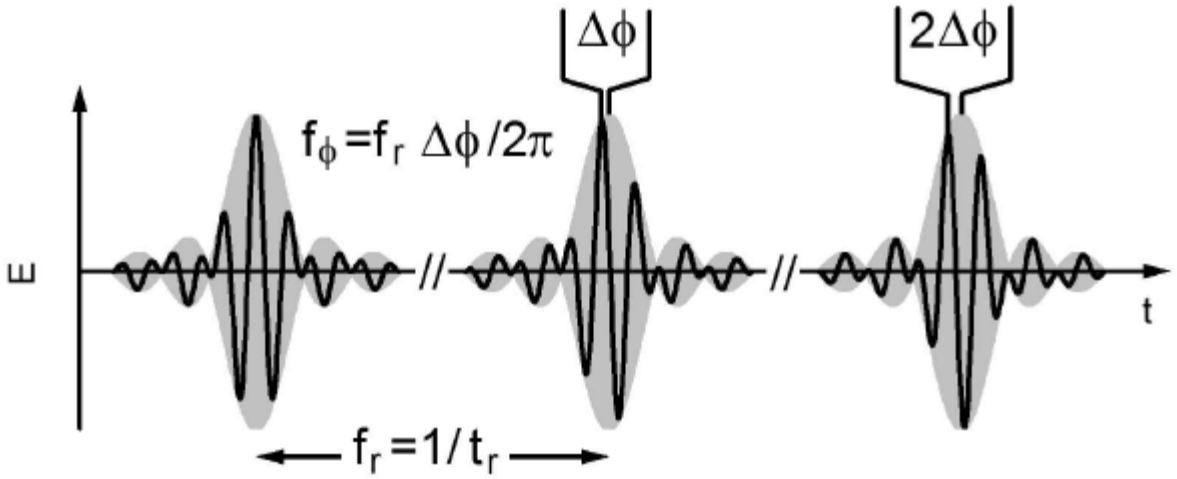


pulse train emitted from mode-locked oscillator

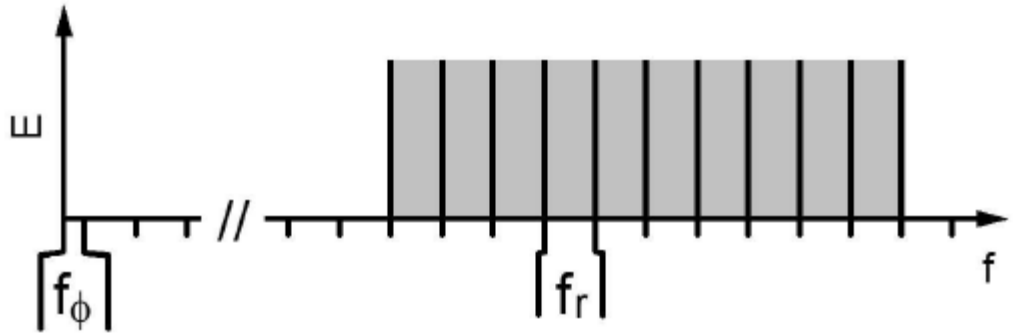


femtosecond frequency comb

$$\omega_m = \frac{2m\pi}{T_r} + \frac{\Delta\varphi}{T_r} = m\omega_r + \omega_{\mathrm{CEO}}$$

$$\nu_m = m\nu_r + \nu_{\mathrm{CEO}}$$

# Active CEP-stabilization of chirped-pulse amplifier

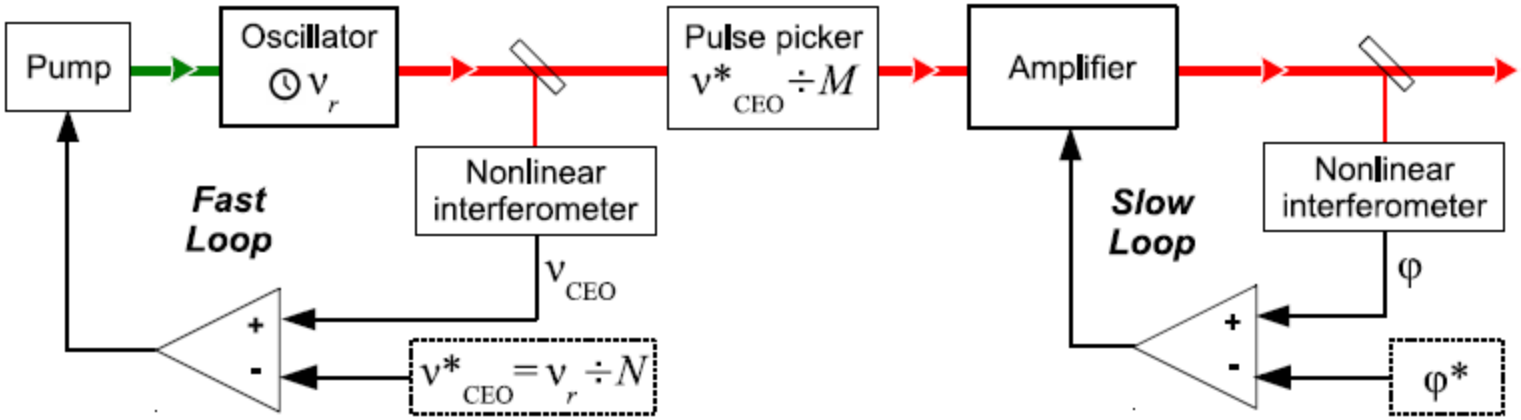


Figure 9.34: Scheme for active CEP stabilization; $\nu^*_{\mathrm{CEO}}$ and $\varphi^*$ are the target values of $\nu_{\mathrm{CEO}}$ and $\varphi$, respectively. From [3]

1. Measure $\nu_{CEO}$ by a nonlinear interferometer
2. Stabilize $\nu_{CEO}$ by an active high-bandwidth feedback on the laser oscillator (fast loop) to $\nu^*_{CEO}$
3. Pick pulses at the integer fraction of $\nu^*_{CEO}$
4. After amplification, measure CEP φ of pulses by a single-shot nonlinear interferometer and use an additional feedback loop (slow loop) to correct for fluctuations induced by the amplification process (and optionally external spectral broadening, e.g., in a hollow-core fiber compressor) and lock CEP to $\varphi^*$.

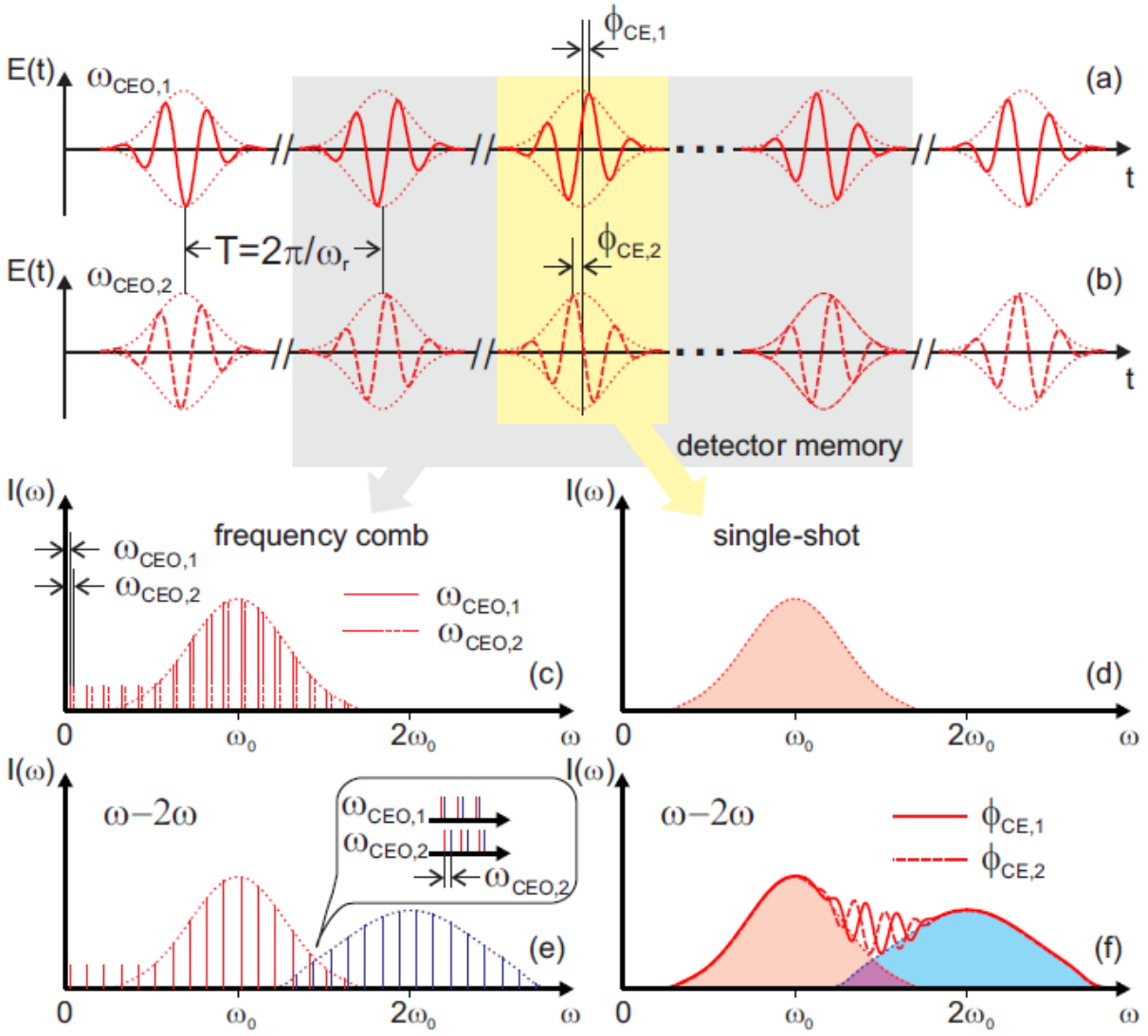


Figure 9.35: Overview of $\omega$-$2\omega$ self-referencing technique in the case of a mode-locked pulse train and an individual laser pulse. (a,b) show a pulse train for two different values of the pulse-to-pulse CEP slip, $\Delta\phi$. (c,d) power spectra of Fourier transforms shown, respectively, for a pulse train "memorized" by the detector and for a single isolated pulse. (e,f) $\omega$-$2\omega$ self-referencing in the overlap region between the fundamental and SF spectra for a frequency comb and a single laser shot. [2]

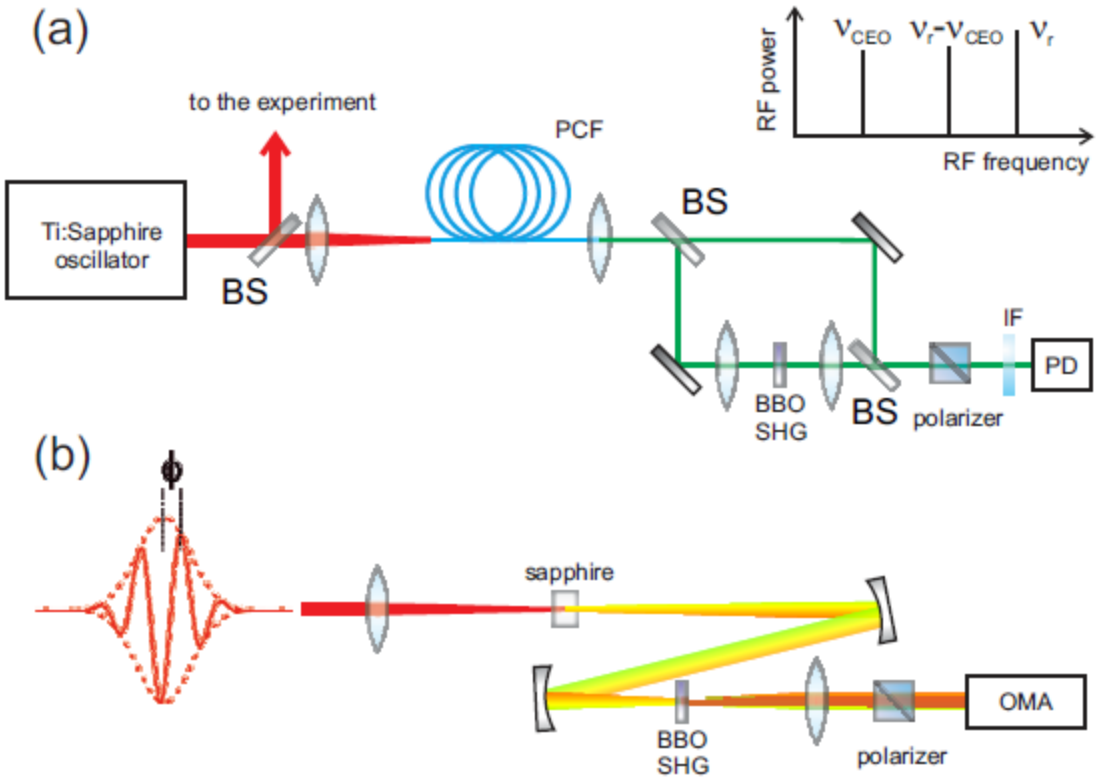


Figure 9.36: (a) $f$-to-$2f$ interferometer setup for measuring the CE frequency from a femtosecond laser oscillator; (b) Inline $f$-to-$2f$ interferometer for measuring the single-shot CEP drift. [2]

$$I(\omega) = I_{FF}(\omega) + I_{SH}(\omega) + 2\sqrt{I_{FF}(\omega)I_{SH}(\omega)}\cos(\omega\tau + \phi) \qquad (9.63)$$

# Phase sum rules of nonlinear processes

three coupled equations in the absence of absorption

$$\begin{cases} \dfrac{\partial A_1}{\partial z} = -j\sigma_1 A_3 A_2^* e^{j\Delta kz} \\ \dfrac{\partial A_2}{\partial z} = -j\sigma_2 A_3 A_1^* e^{j\Delta kz} \\ \dfrac{\partial A_3}{\partial z} = -j\sigma_3 A_1 A_2 e^{-j\Delta kz} \end{cases} \tag{9.65}$$

where $\sigma_i$ are the nonlinear coupling coefficients, and $\Delta k = k_3 - k_2 - k_1$ is the phase mismatch. Introducing $A_i = B_i \exp(j\varphi_i)$, where $B_i = |A_i|$ are the amplitudes and $\varphi_i$ are the phases of the respective waves, the real and imaginary parts of Eq. (9.65) are transformed to:

$$\begin{cases} \dfrac{\partial B_1}{\partial z} = \sigma_1 B_2 B_3 \sin\Psi \\ \dfrac{\partial B_2}{\partial z} = \sigma_2 B_1 B_3 \sin\Psi \\ \dfrac{\partial B_3}{\partial z} = -\sigma_3 B_1 B_2 \sin\Psi \\ \dfrac{\partial \Psi}{\partial z} = \Delta k + \left(\sigma_1 \dfrac{B_2 B_3}{B_1} + \sigma_2 \dfrac{B_1 B_3}{B_2} - \sigma_3 \dfrac{B_1 B_2}{B_3}\right) \cos\Psi \end{cases} \tag{9.66}$$

where $\Psi = \varphi_3 - \varphi_2 - \varphi_1 + \Delta kz$ is the so-called generalized phase. Assuming perfect phase matching, $\Delta kz = 0$, system (9.66) leads to simple solutions for different boundary conditions. In the following, we discuss the phase sum rules

Let's first consider the case of sum-frequency generation (SFG), i.e., the generation of a field at $\omega_3 = \omega_1 + \omega_2$: assuming the boundary condition $B_3(z = 0) = 0$, the value of the generalized phase that maximizes the right-hand side in the third equation in (9.66) is $\Psi = -\pi/2$, which corresponds to the SFG phase $\varphi_{\mathrm{SFG}} = \varphi_3 = \varphi_1 + \varphi_2 - \pi/2$ (see Fig. 9.37(a)). For the case of SHG of a field at the fundamental frequency (FF), which is a degenerate SFG process with $\omega_1 = \omega_2 = \omega_{\mathrm{FF}}$ and $\omega_3 = \omega_{\mathrm{SH}} = 2\omega_{\mathrm{FF}}$, we get $\varphi_{\mathrm{SH}} = 2\varphi_{\mathrm{FF}} - \pi/2$. Let's now consider the case of difference-frequency generation (DFG), which is equivalent to the process of idler generation in an OPA, i.e., $\omega_2 = \omega_3 - \omega_1$: assuming the boundary condition $B_2(z = 0) = 0$, the value of the generalized phase that maximizes the right-hand side term in the second equation in (9.66) becomes $\Psi = \pi/2$. Consequently, $\varphi_{\mathrm{DFG}} = \varphi_2 = \varphi_3 - \varphi_1 - \pi/2$ (Fig. 9.37(b)). A very similar effect occurs in the third-order nonlinear process of four-wave mixing (FWM), in which four waves at frequencies $\omega_1$, $\omega_2$, $\omega_3$ and $\omega_4$, with

$\omega_4 = \omega_1 - \omega_2 + \omega_3$, are coupled in a third-order nonlinear medium. The CEPs of the waves are linked by the relationship: $\varphi_4 = \varphi_1 - \varphi_2 + \varphi_3 - \pi/2$ (Fig. 9.37(c)). Self-phase modulation (SPM), i.e., spectral broadening due to the instantaneous intensity-dependent variations of index of refraction in a Kerr medium, can be regarded as a special case of FWM, in which a new frequency $\omega_{\mathrm{SPM}}$ is generated starting from three frequencies $\omega_1$, $\omega_2$ and $\omega_3$, all belonging to the pulse spectrum, by the FWM process $\omega_{\mathrm{SPM}} = \omega_1 - \omega_2 + \omega_3$. These new frequencies in turn contribute to subsequent FWM processes, causing a progressive broadening of the pulse spectrum as it propagates through the nonlinear medium. If we now consider that the mixing frequencies belong to the same beam and hence share the same CEP $\varphi_1 = \varphi_2 = \varphi_3 = \varphi$, then the SPM pulse will have the CEP $\varphi_{\mathrm{SPM}} = \varphi_1 - \varphi_2 + \varphi_3 - \pi/2 = \varphi - \pi/2$. This demonstrates that, net $\pi/2$, the newly added frequency components of the broadened SPM spectrum inherit the original value of the CEP of the driving pulse. The SPM/FWM process is the dominant nonlinear interaction behind the spectral broadening in gas-filled hollow waveguides and in gas filaments and white-light continuum (WLC) generation in bulk materials.

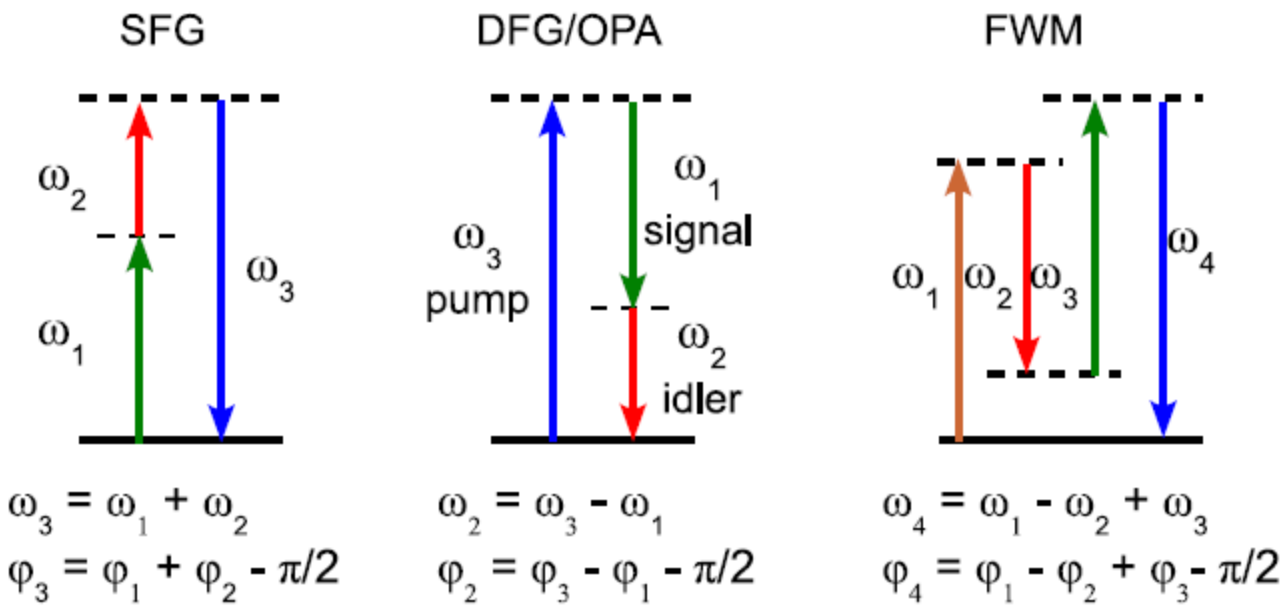


Figure 9.37: Frequency and phase summation rules for (a) sum-frequency generation (SFG), (b) difference-frequency generation (DFG), equivalent to the generation of the idler wave in an OPA, and (c) four-wave mixing (FWM) process. From [2]

# Passive stabilization of the CEP

The passive method is an alternative *all-optical* approach for the generation of CEP-stable pulses. If a DFG process $\omega_{DF} = \omega_2 - \omega_1$ occurs between two pulses with the same shot-to-shot CEP fluctuations $\varphi$, so that $\varphi_1 = \varphi$ and $\varphi_2 = \varphi + c$, then $\varphi_{DF} = \varphi_2 - \varphi_1 - \pi/2 = c - \pi/2 = const.$, *i.e.*, the fluctuations of $\varphi$ are automatically cancelled. Passive CEP stabilization has some clear advantages with respect to the active one: (i) being an all-optical technique, it does not require any electronic feedback circuits imposing bandwidth limitations; (ii) it directly produces a train of CEP-stable pulses, avoiding the need to pick pulses at a fraction of $\nu_{CEO}$.

# Passive stabilization of the CEP

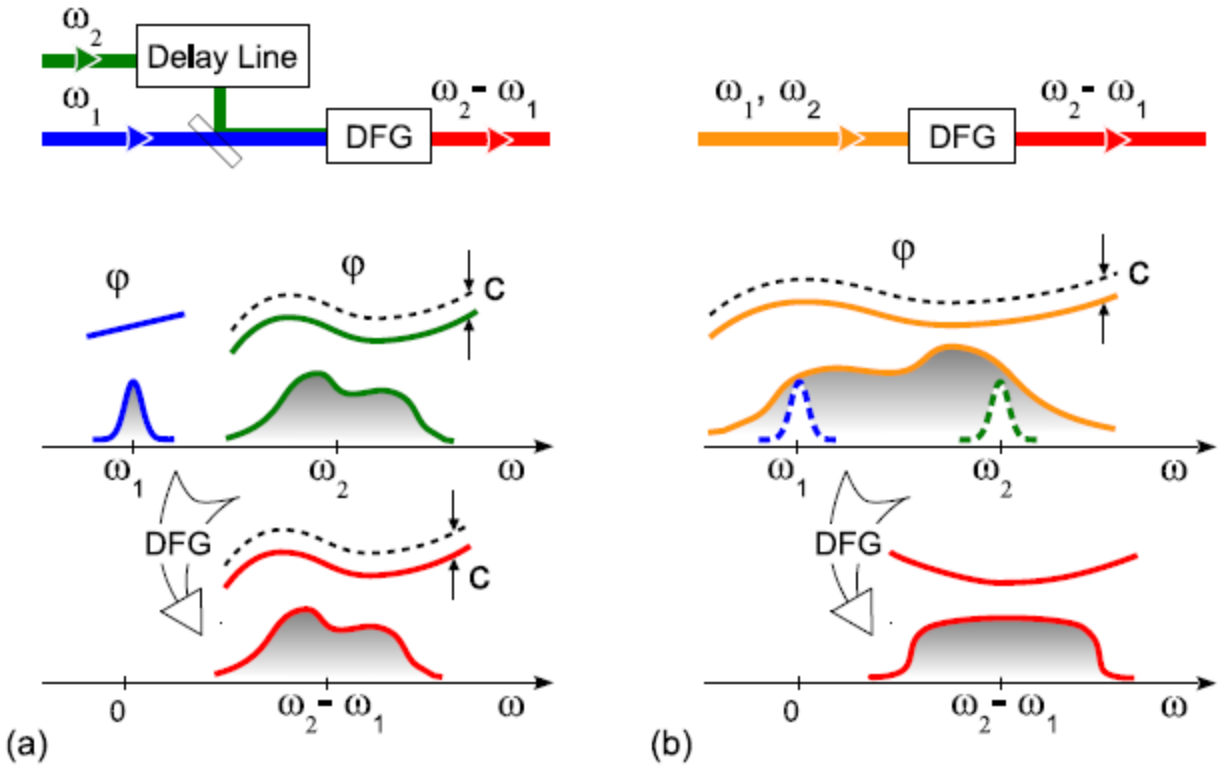


Figure 9.38: Comparison of (a) inter-pulse and (b) intra-pulse stabilization schemes. Lower panels provide the evolution of both intensity and phase in the frequency domain; $\varphi$ is the absolute phase, c denotes fluctuations of the CEP. From [3]

# Passive stabilization of the CEP

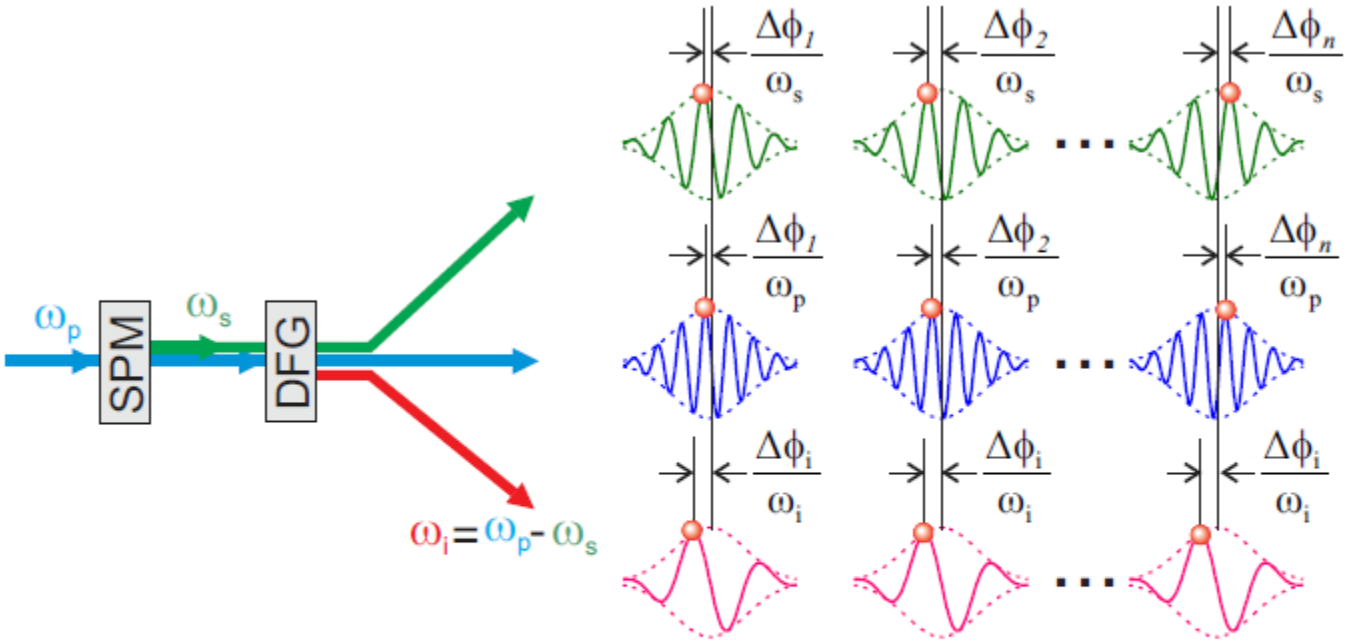


Figure 9.39: Cartoon illustrating passive CEP-stabilization of the idler: if the seed of the OPA is obtained by SPM from the pump pulses, any shot-to-shot phase fluctuations in the pump and signal pulses cancel out in the idler, yielding shot-to-shot reproducible phase-stable idler pulses. From [2]

# 9.10.2 Generation of CEP-stable pulses from an OPA

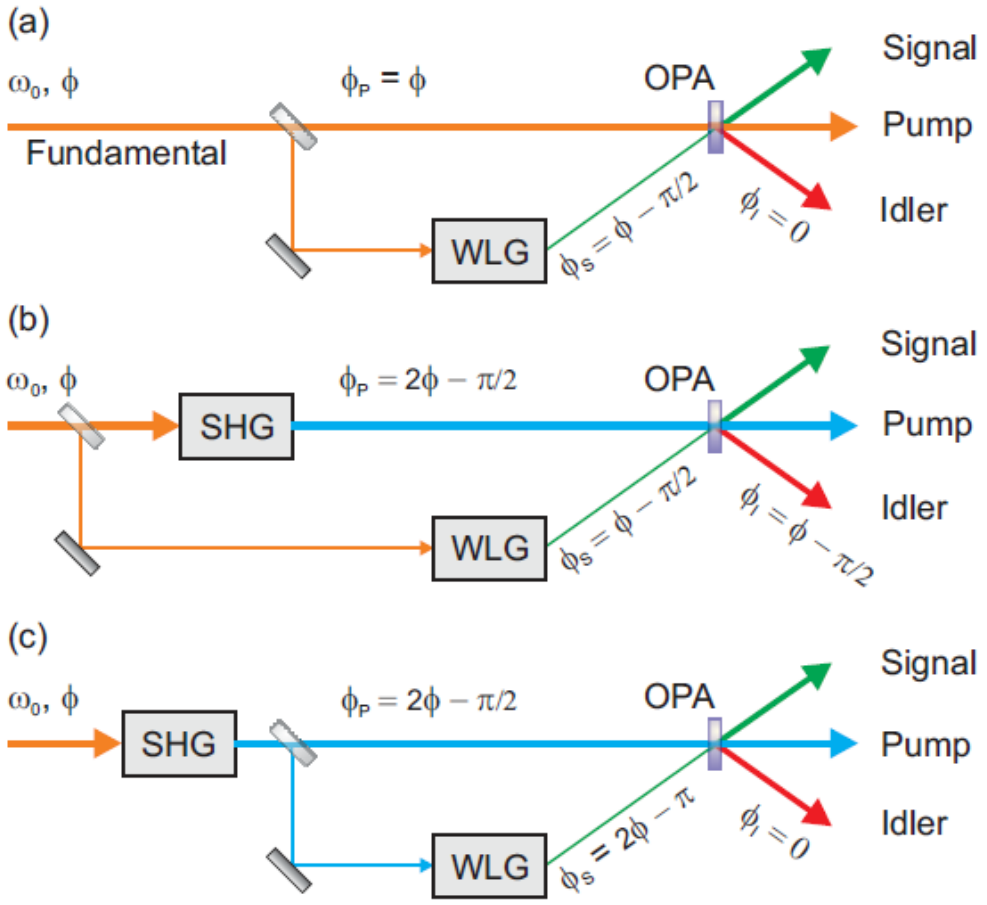


**CEP-stable idler**

**'phase-repeating OPA'**

**CEP-stable idler**

Figure 9.40: Schematics of three OPA configurations. For clarity, the seed and the pump beams are shown to intersect non-collinearly in the crystal. However, the conclusions are also valid for the collinear beam arrangement. From [2]

One important note of caution: As can bee seen from the equation system (9.66), from the standpoint of the passive CEP-stabilization technique discussed here, we note that pre-existence of an input field (seed) at the desired DFG (idler) frequency $\omega_2 = \omega_3 - \omega_1$ has to be strictly avoided! On the one hand, it changes the value of the phase lag. More significantly, it corresponds to the opening of a competing channel (the case of double seeding) which would result in the generation of an idler wave at the signal frequency $\omega_1$ causing unintended interference with the seed at $\omega_1$.

The above considerations are valid when the OPA is seeded by WLC, which inherits the CEP of the driving pulse. For parametric superfluorescence (PSF), which is initiated by vacuum fluctuations or quantum noise, one expects that the CEP link between the pump and the PSF pulses is completely lost; this has indeed been verified, both numerically and experimentally, in [20]. For this reason, an OPA seeded by PSF cannot be used in any passive CEP-stabilization scheme. It should be noted that, for a multi-stage OPA driven by a sufficiently intense pump, efficient amplification of PSF with random CEP takes place even in the absence of a seed beam. This mechanism can compete with the amplification of the WLC seed causing extra CEP jitter and even excessive amplitude noise. Therefore, to suppress the parasitic amplification of PSF, the pump intensity and the gain of each OPA stage should be carefully optimized.

# CEP-stable pulses from a visible NOPA

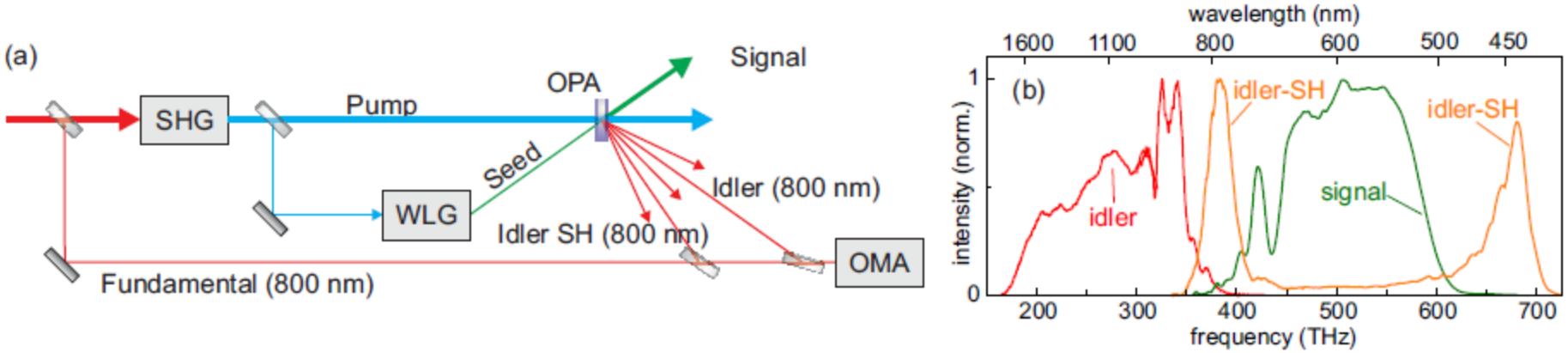


Figure 9.41: Schematic of experimental setup for CEP self-stabilization measurement. (a) NOPA and three-beam interferometer. OMA: Optical Multichannel Analyzer. (b) Output spectra of the NOPA. Note the spectral overlap between the idler and its SH around 790 nm. [2]

A. Baltuška, T. Fuji, and T. Kobayashi, Phys. Rev. Lett. **88**, 133901 (2002)

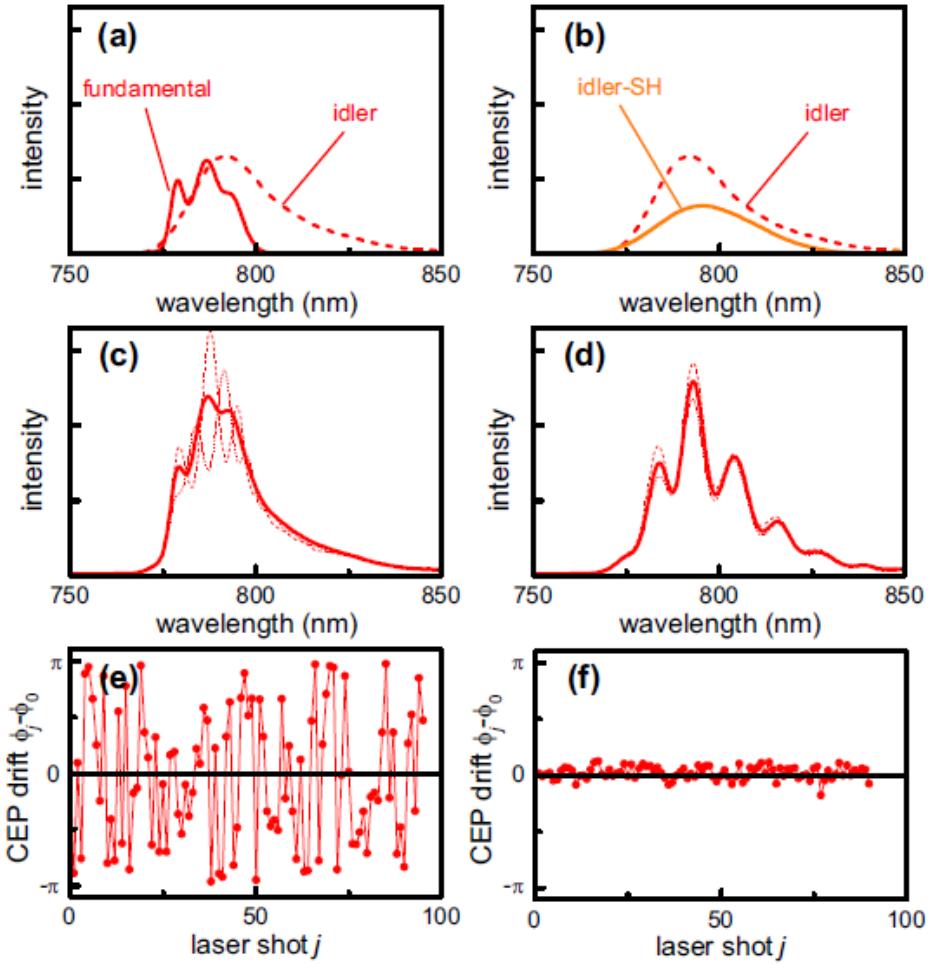


Figure 9.42: Experimental results of CEP self-stabilization measurement. (a,b) Overlapped spectral portions of the residual fundamental, idler, and idler-SH beams. (c,d) Solid curves show interference pattern averaged over 1000 shots, whereas dotted curves represent single-shot interferograms. (e,f) Dots show relative CEP jumps wrapped on a $[-\pi, +\pi]$ interval. Note that the stable phase pattern obtained from the interference of the idler and its second harmonic is a direct proof of CEP self-stabilization. [2]

A. Baltuška, T. Fuji, and T. Kobayashi, Phys. Rev. Lett. **88**, 133901 (2002)

# CEP-stable ultrabroadband pulses from cascaded OPAs

(i) an FF-pumped, WLC-seeded near-IR OPA, generating narrowband, CEP-stable idler pulses; (ii) a WLC generation stage driven by the idler, producing a CEP-stable seed; (iii) a broadband OPA stage seeded by the spectrally broadened idler. The OPA preserves the absolute phase stability of the seed and produces ultrabroadband tunable pulses with $\mu$J-level energy; scaling of the source energy by the addition of subsequent amplification stages is straightforward.

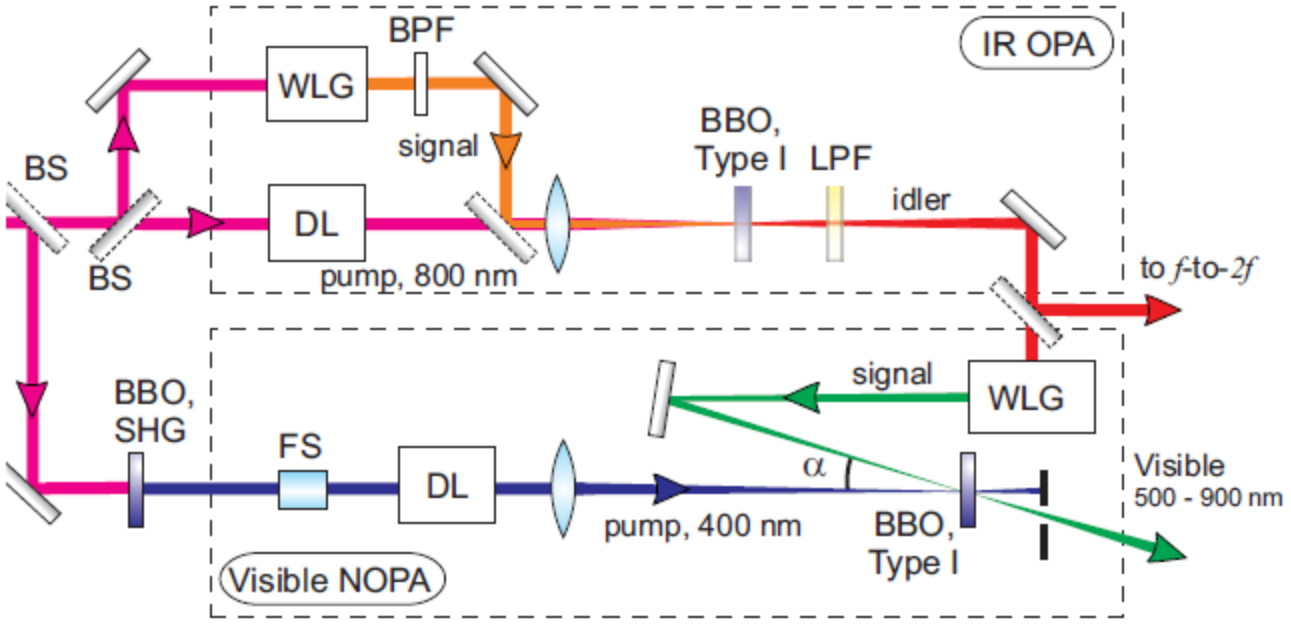


Figure 9.43: Experimental setup for the generation of self-phase-stabilized pulses in the visible. BS, beam splitters; DL, delay lines; WLG, white-light generation stages; LPF, long-pass filter; BPF, bandpass filter; FS, fused silica glass block. [2]

C. Manzoni *et al.*, Appl. Phys. Lett. 90, 171111 (2007)

# CEP-stable ultrabroadband pulses from cascaded OPAs

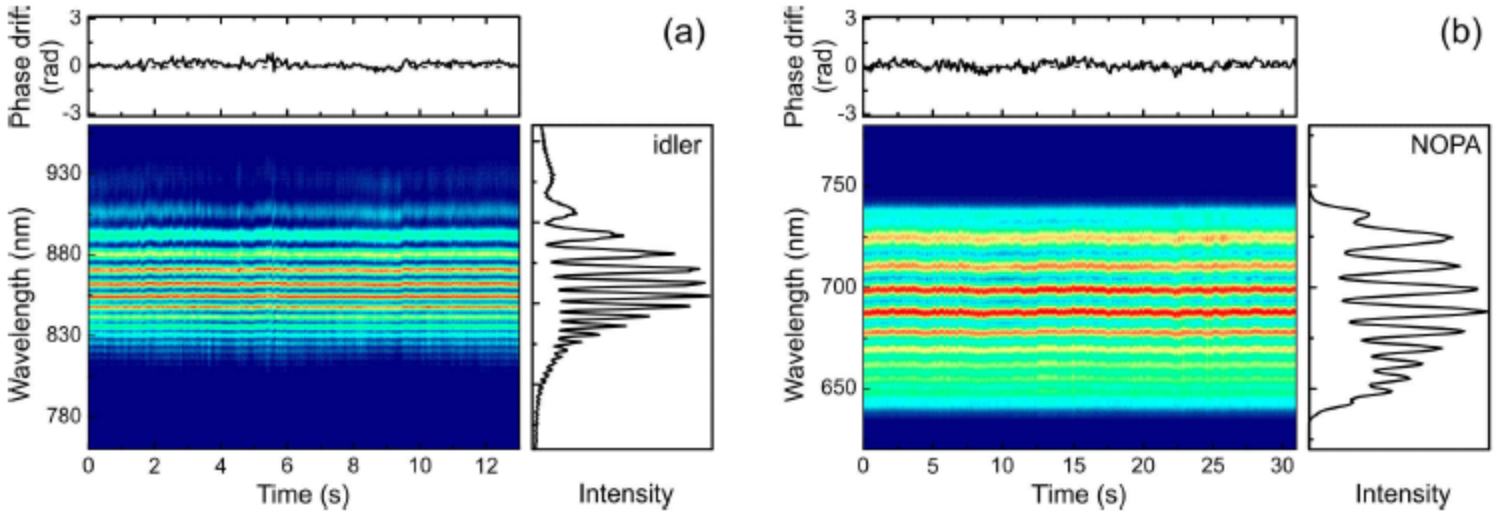


Figure 9.44: (a) $f$-to-$2f$ interferometric characterization of idler pulses from the IR OPA. Upper panel: deduced CEP evolution, indicating a fluctuation with rms $\Delta\phi$=0.19 rad. Left panel: sequence of interferograms acquired for 13 seconds. Right panel: fringe pattern obtained averaging over 10 laser shots. (b) same as (a), but for the visible NOPA pulses. A fluctuation with rms $\Delta\phi$=0.23 rad is obtained. [2]

C. Manzoni *et al.*, Appl. Phys. Lett. 90, 171111 (2007)

# CEP-stable ultrabroadband pulses from cascaded OPAs

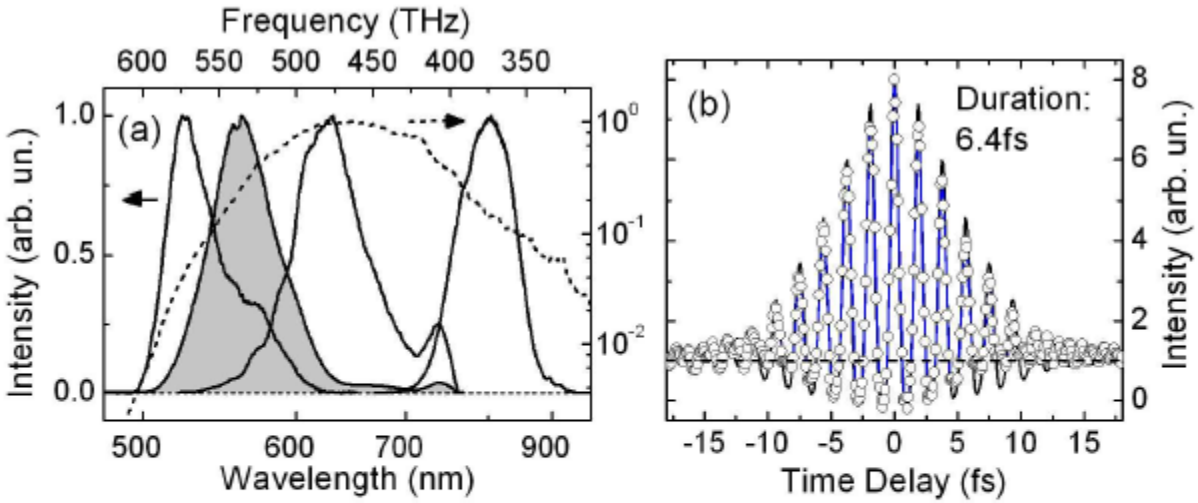


Figure 9.45: (a) Dashed line, logarithmic scale: WLC generated by the IR OPA idler and seeding the visible NOPA. Solid line: sequence of spectra obtained tuning the visible NOPA. (b) Interferometric autocorrelation trace (circles) of a pulse centered at 550nm [shaded spectrum of panel (a)]; the best fit to the experimental data (solid line) indicates a 6.4-fs pulse duration, close to the TL. [2]

C. Manzoni *et al.*, Appl. Phys. Lett. 90, 171111 (2007)

# CEP-stable IR pulses from hybrid type-II OPCPA/ filamentation system

**building blocks:**

(i) self-CEP-stabilized 1.5-µm frontend:
CEP-stable collinear type-I BBO OPA + narrowband type-II KTP OPA
(ii) type-II KTP OPCPA based on picosecond Nd:YAG technology
(iii) pulse self-compression by filamentation in noble gases

**motivation for architecture:**

(a) near-degenerate type-I OPAs have worst possible quantum defect for signal
(b) even though group-velocity-matched OPAs deliver ultrabroad output spectra (>200 nm), quality of resulting compressed pulses most often remains poor due to intrinsically steep slopes of the parametrically amplified spectra
(c) more narrowband amplification has the advantage of optimizing the spectral brightness of the signal (suppression of parametric superfluorescence)
(d) when scaling the pulse energies of type-I OPAs to the mJ-level, cascaded FWM can cause unwanted losses due to parasitic self-diffraction.

O. D. Mücke *et al.*, Opt. Lett. **34**, 118-120 (2009)

O. D. Mücke *et al.*, Opt. Lett. **34**, 2498-2500 (2009)

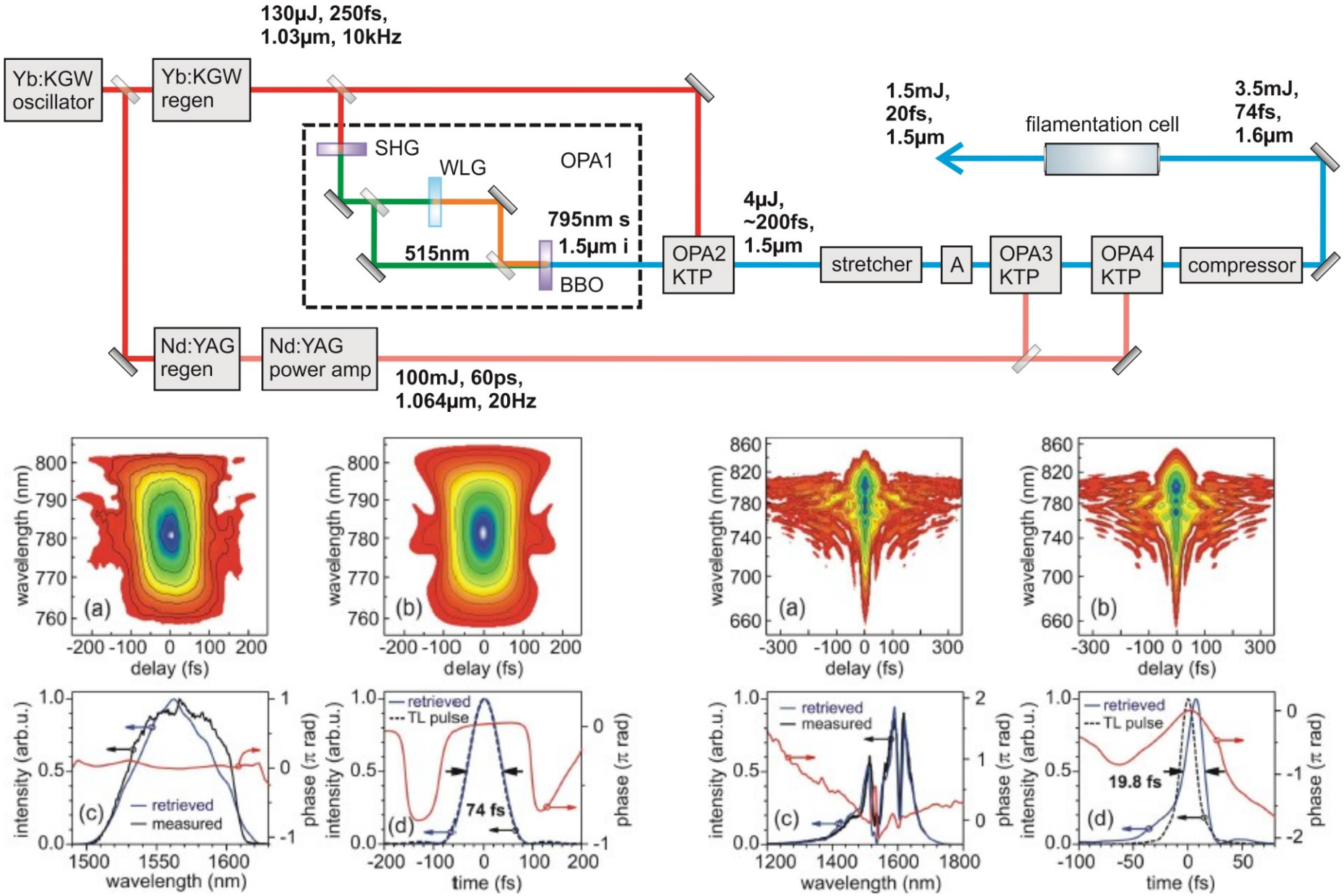


O. D. Mücke *et al.*, Opt. Lett. **34**, 118-120 (2009)

O. D. Mücke *et al.*, Opt. Lett. **34**, 2498-2500 (2009)

# OPCPA of a 2-μm seed obtained by intrapulse DFG

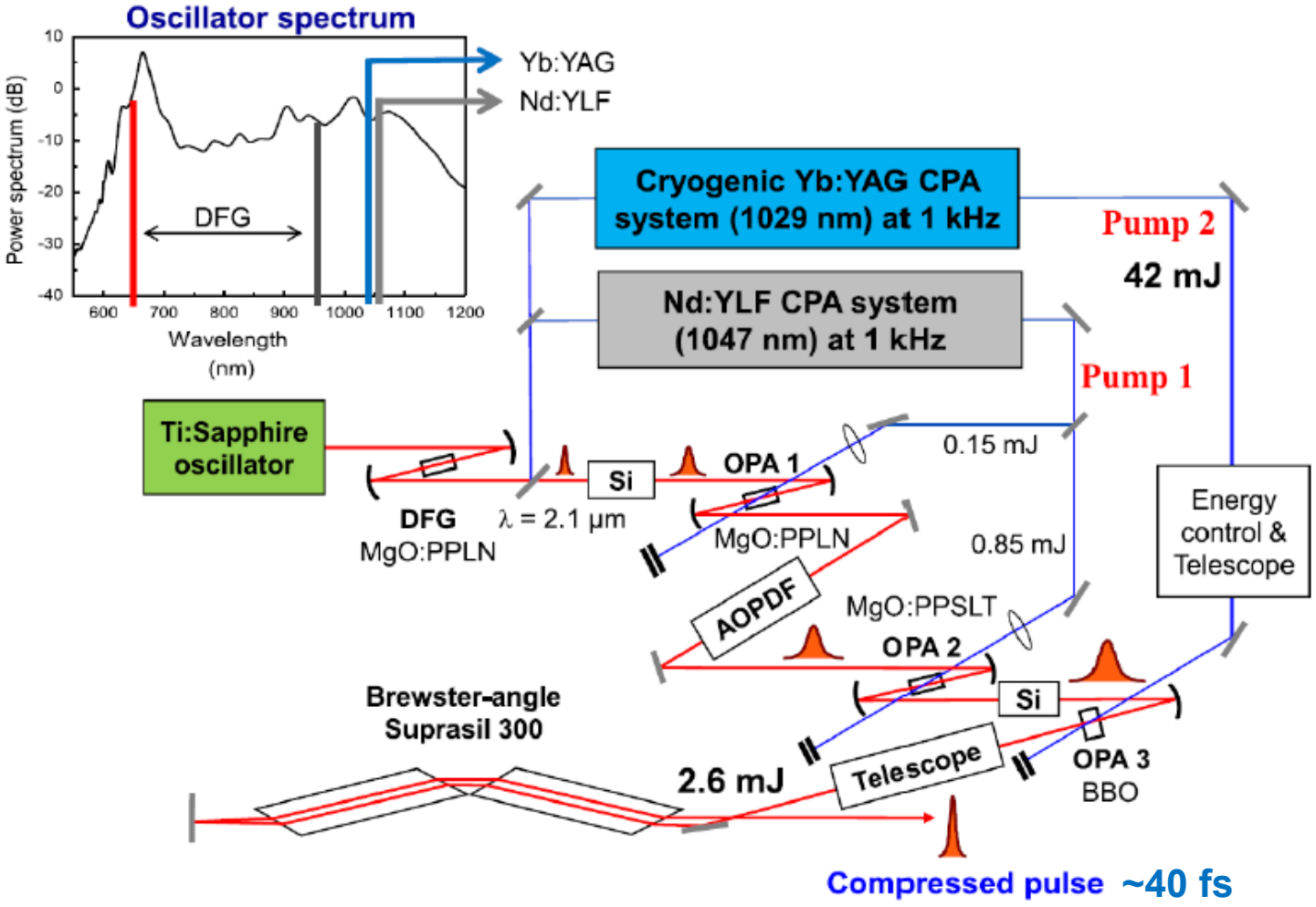



K.-H. Hong *et al.*, Opt. Lett. **39**, 3145 (2014)

K.-H. Hong *et al.*, Opt. Express **19**, 15538 (2011)

J. Moses *et al.*, Opt. Lett. **34**, 1639 (2009)

at MPQ: T. Fuji *et al.*, Opt. Lett. **31**, 1103 (2006); X. Gu *et al.*, Opt. Express **17**, 62 (2009); Y. Deng *et al.*, Opt. Lett. **37**, 4973 (2012).

# Dual-chirped IR optical parametric amplification

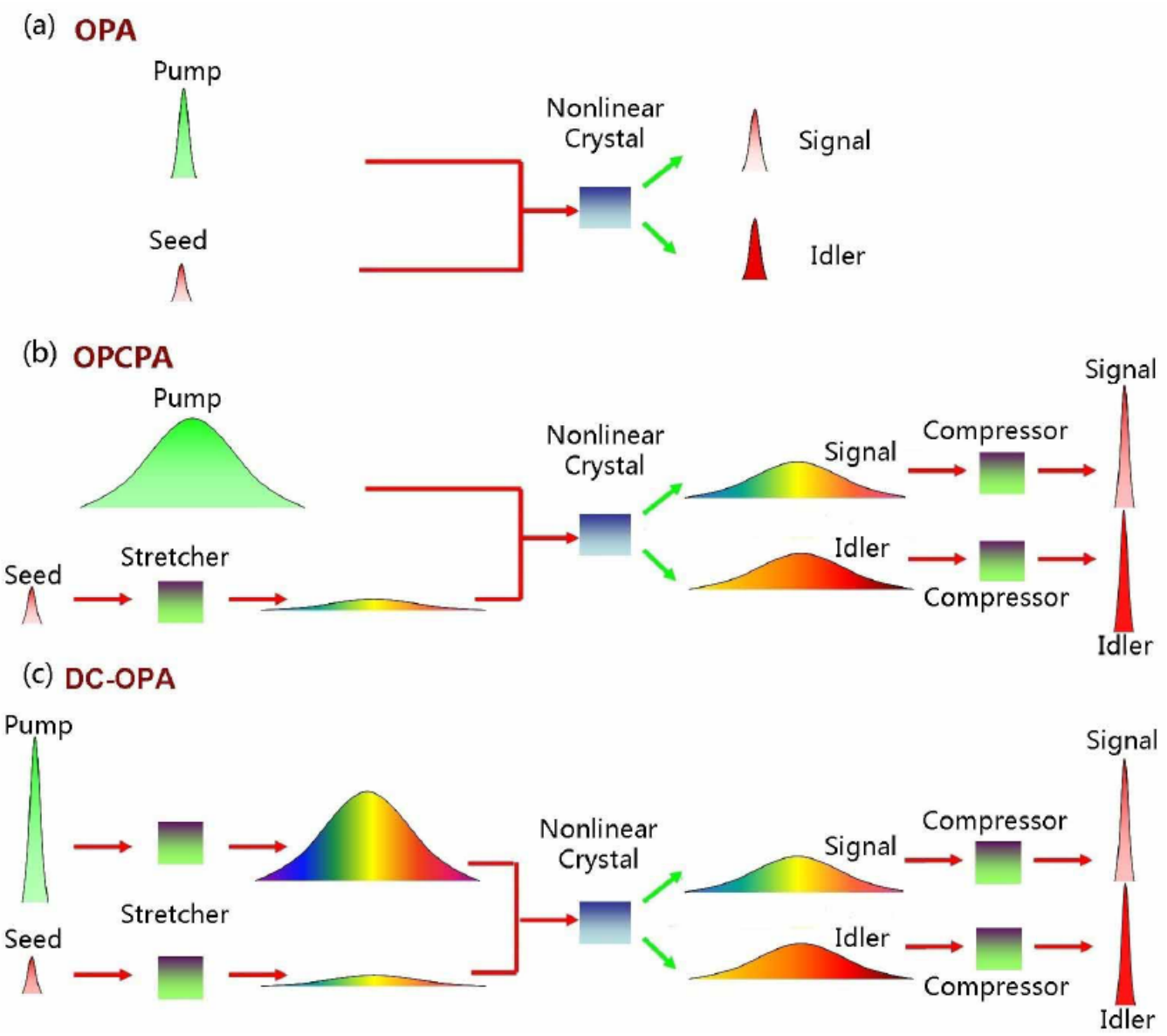


Q. Zhang *et al.*, Opt. Express **19**, 7190-7212 (2011)

# Dual-chirped IR optical parametric amplification

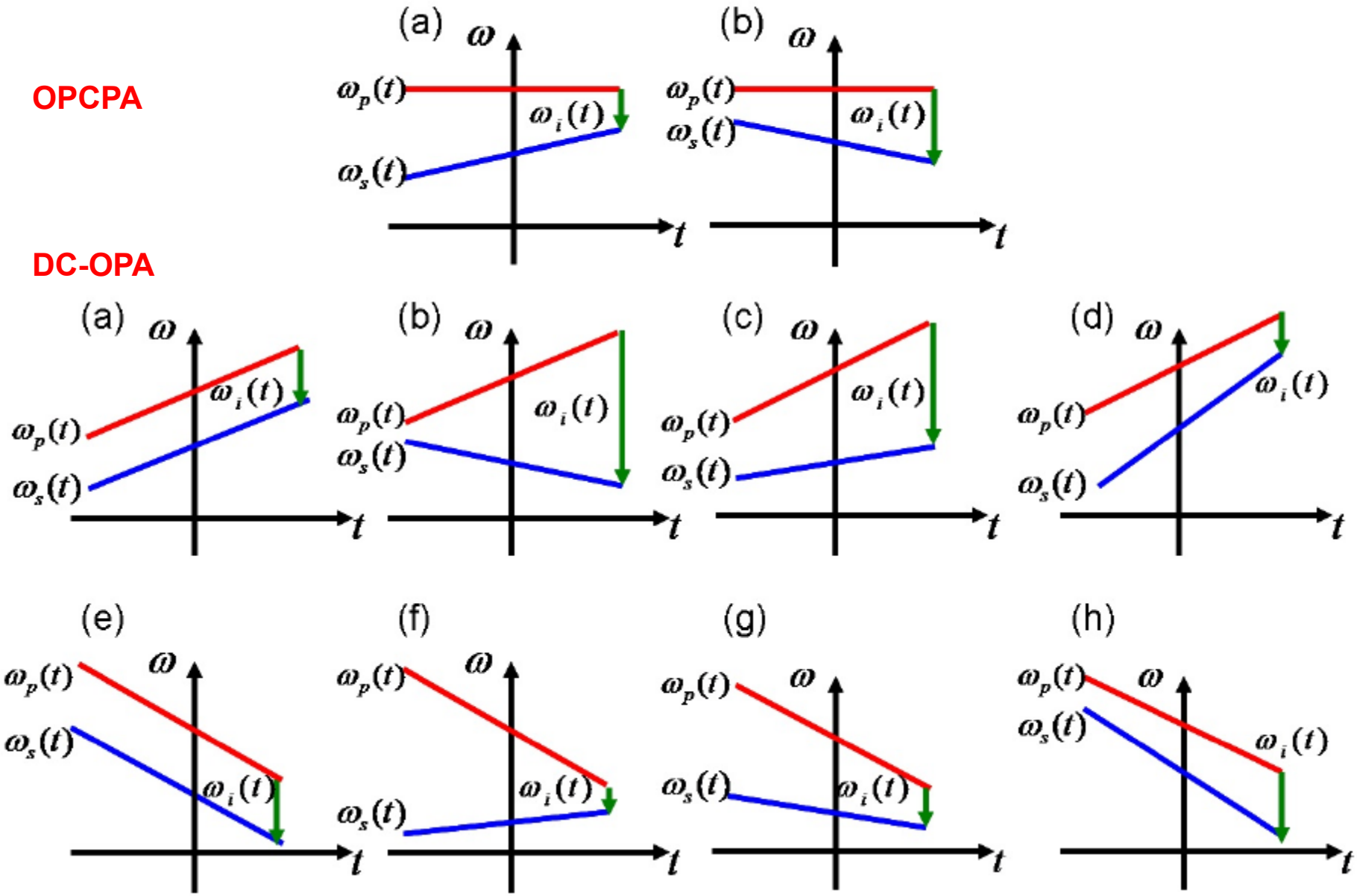


Q. Zhang *et al.*, Opt. Express **19**, 7190-7212 (2011)

# Dual-chirped IR optical parametric amplification

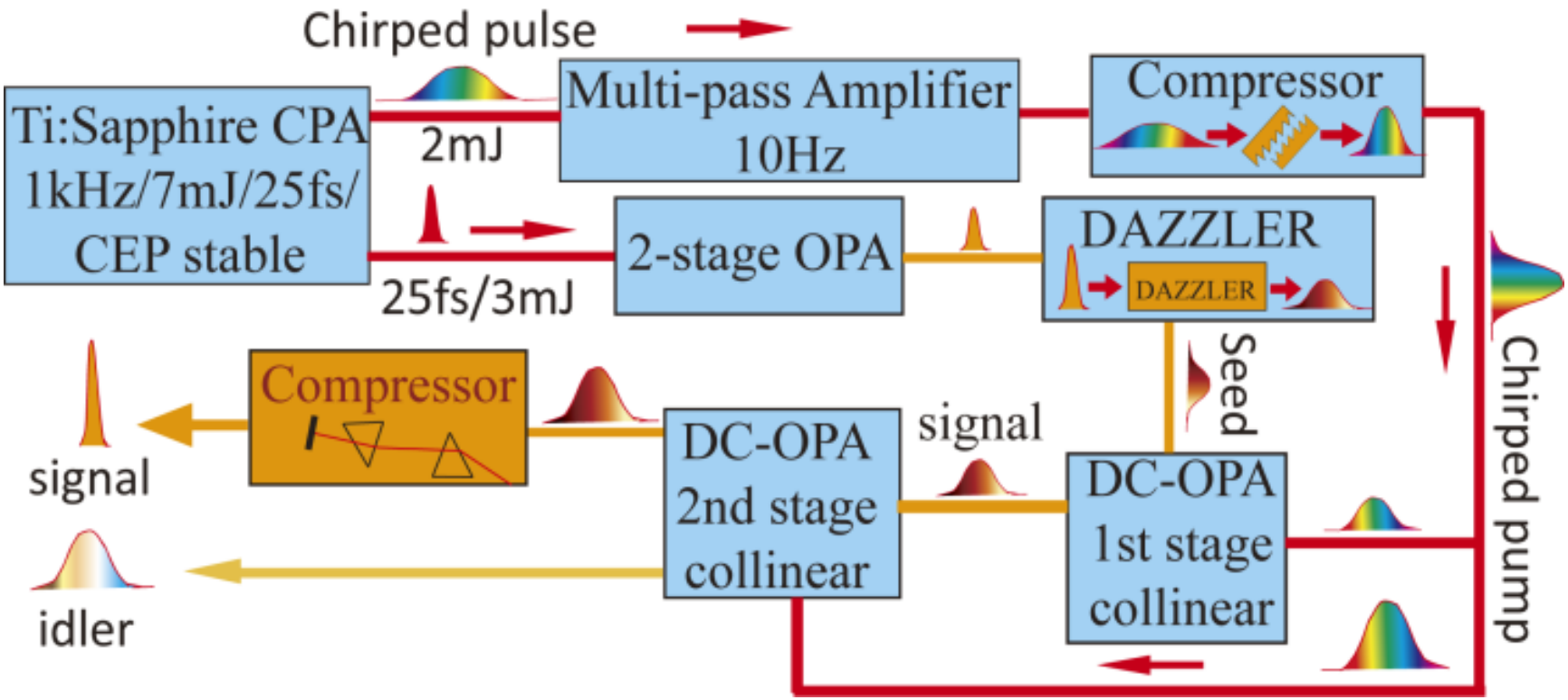


Y. Fu *et al.*, Opt. Lett. **21**, 5082-5085 (2015)

Y. Fu *et al.*, J. Opt. **17**, 124001 (2015)

Y. Yin *et al.,* Sci. Rep. **7**, 45794 (2017) 4-12 μm ZGP DC-OPA

Y. Fu *et al.*, Sci. Rep. **8**, 7692 (2018) multi-TW IR, scaling to 10J/PW level

Y. Fu *et al.,* Appl. Phys. Lett. **112**, 241105 (2018) 31 mJ, 3.3 μm, $MgO:LiNbO_3$

# Dual-chirped IR optical parametric amplification

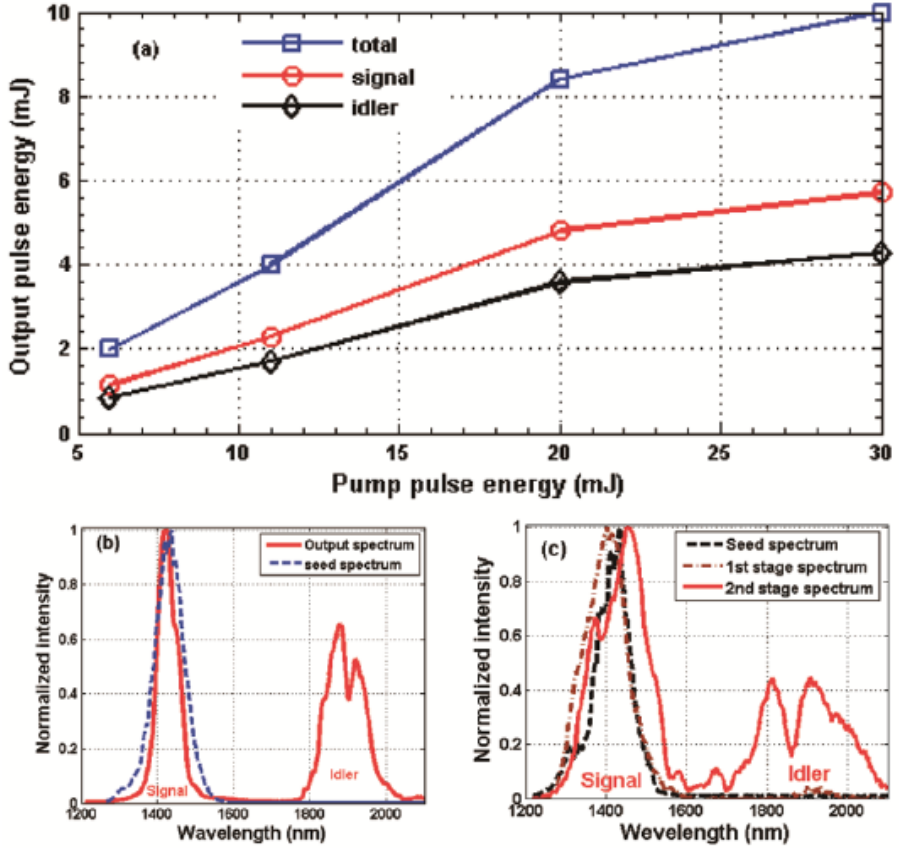


30%-40% total (=s+i) efficiency

pump at 100-mJ level

signal compressed to 27fs

self-CEP-stabilized idler

good prospects for scaling to hundred-mJ-level and even J-level

Figure 9.53: (a) Energy scalability experimentally confirmed by a single-stage DC-OPA. Blue solid-square, total output energy; red solid-circular, signal pulse energy; black solid-rhombic, idler pulse energy. (b) Typical seed (blue dashed) and output (red solid) spectra corresponding to panel (a). (c) Spectra for 80 mJ pumping in a two-stage DC-OPA. Black dashed curve, seed spectrum; brown dash-dotted curve, signal spectrum after first stage; red solid curve, spectrum after second stage. [32]

Y. Fu *et al.*, Opt. Lett. **21**, 5082-5085 (2015)

Y. Fu *et al.*, J. Opt. **17**, 124001 (2015)

# Parametric sub-cycle optical waveform synthesizers

- >2-octave-wide waveform synthesis from OPAs at the multi-mJ level and at 1 kHz
- WLG seed split into 3 wavelength channels and amplified in 3 OPA stages each
- 3 channels are individually compressed and coherently recombined
- relative timing is tightly locked using balanced optical cross-correlators (BOCs)

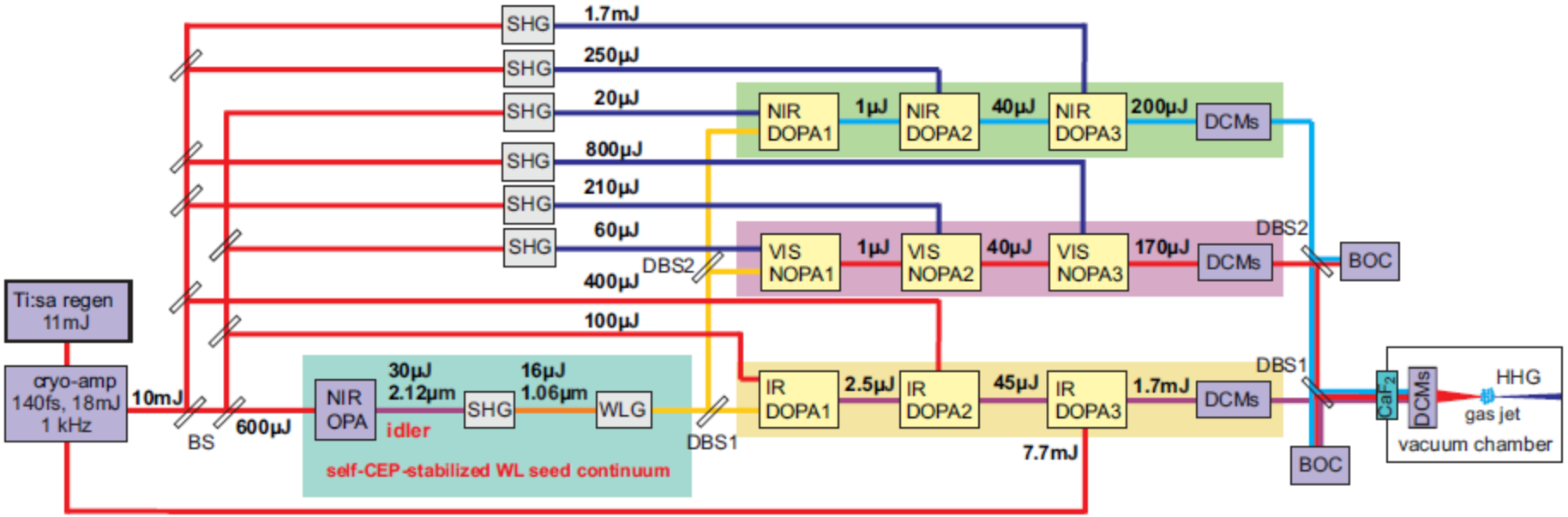


NOPA: noncollinear OPA; DOPA: degenerate OPA


O. D. Mücke *et al.*, IEEE J. Sel. Top. Quantum Electron. **21**, 8700712 (2015)
C. Manzoni *et al.*, Laser & Photonics Rev. **9**, 129-171 (2015)

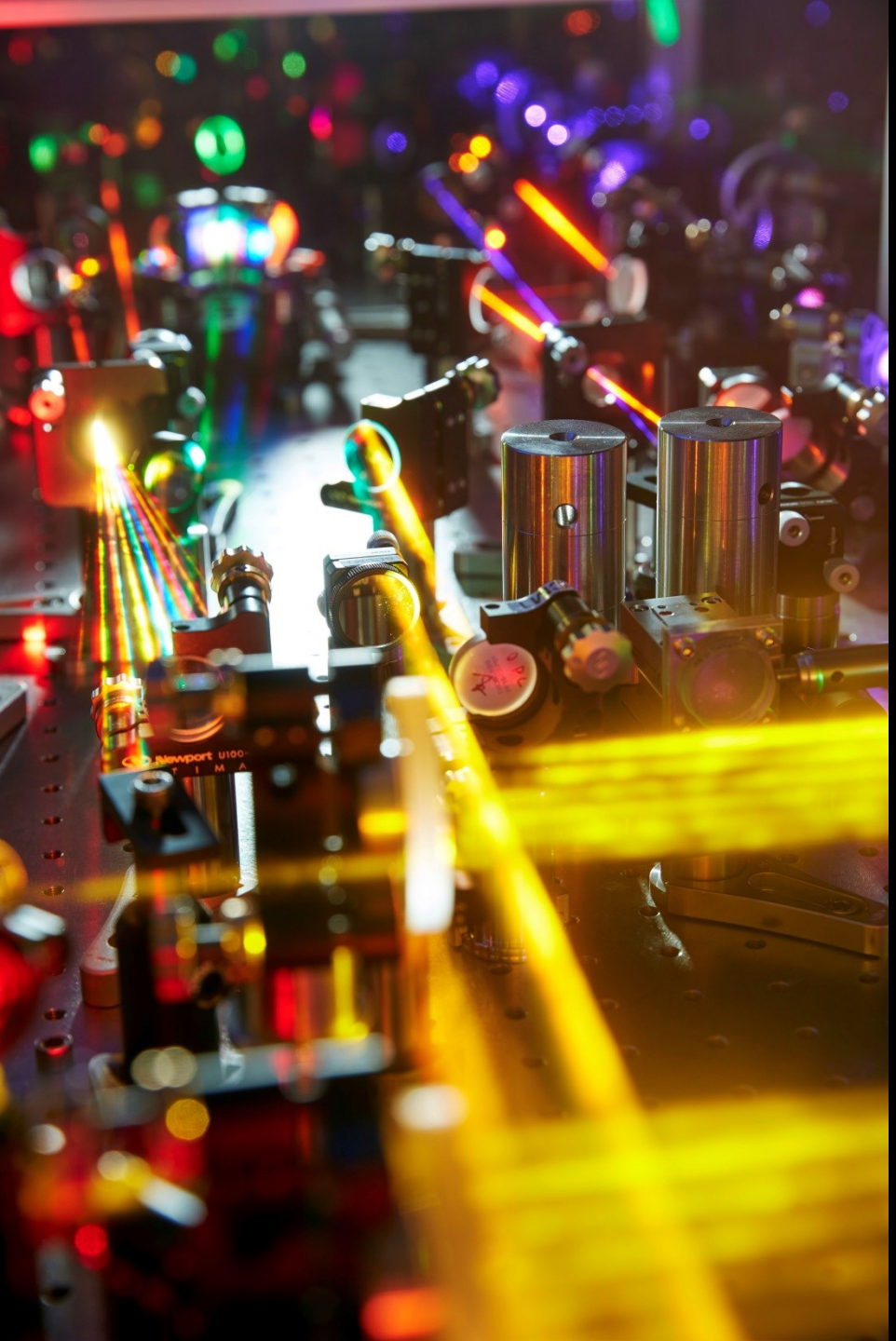
Newport

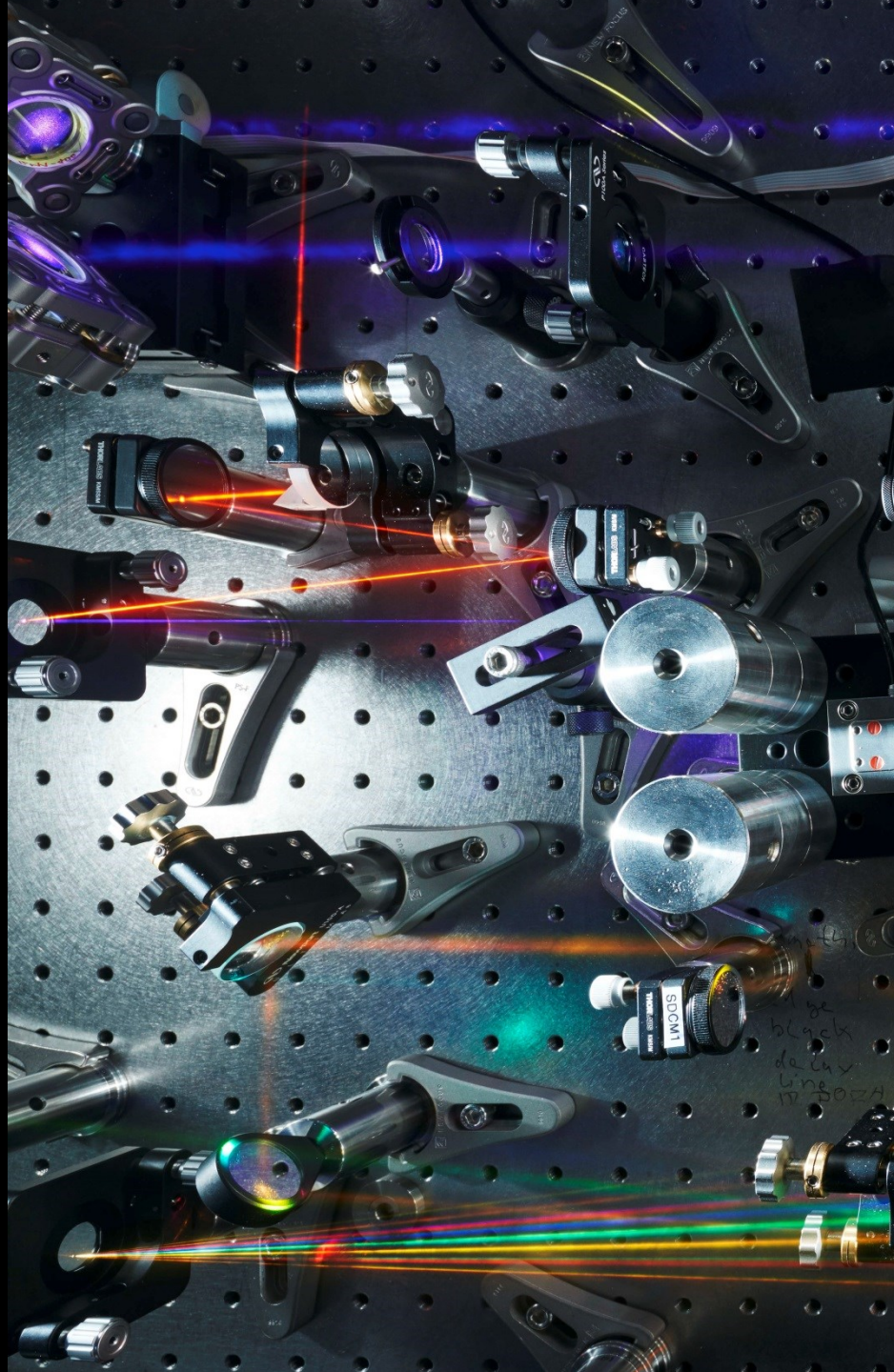
SDCM1

# Parametric sub-cycle optical waveform synthesizers

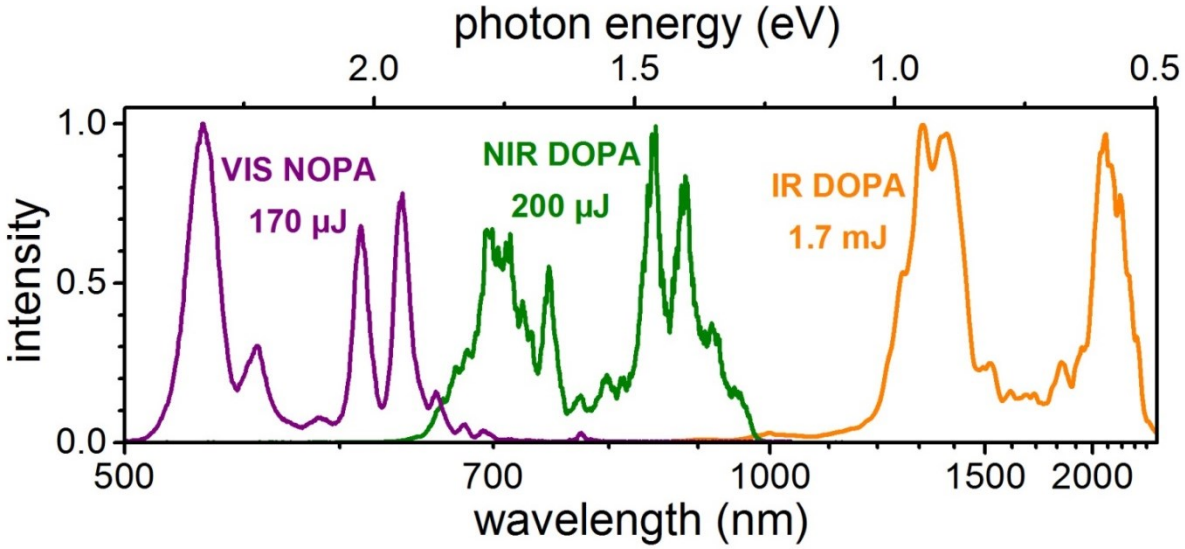


| VIS NOPA | NIR DOPA | IR DOPA |
|---|---|---|
| **0.17 mJ signal** | **0.20-0.25 mJ signal** | **1.7 mJ octave-spanning signal** |
| **20%** (0.8 mJ pump) pump-signal conversion efficiency | **12-15%** (1.7 mJ pump) pump-signal conversion efficiency | **22%** (7.7 mJ pump) pump-signal conversion efficiency |
| TL 5.6 fs | TL 5.2 fs | TL 5.2 fs |
| 2.9 optical cycles @ $\lambda_c$=573nm | 2.1 optical cycles @ $\lambda_c$=750nm | **1.1** optical cycle @ $\lambda_c$=1.4um |

O. D. Mücke *et al.*, IEEE J. Sel. Top. Quantum Electron. **21**, 8700712 (2015)

# Parametric sub-cycle optical waveform synthesizers

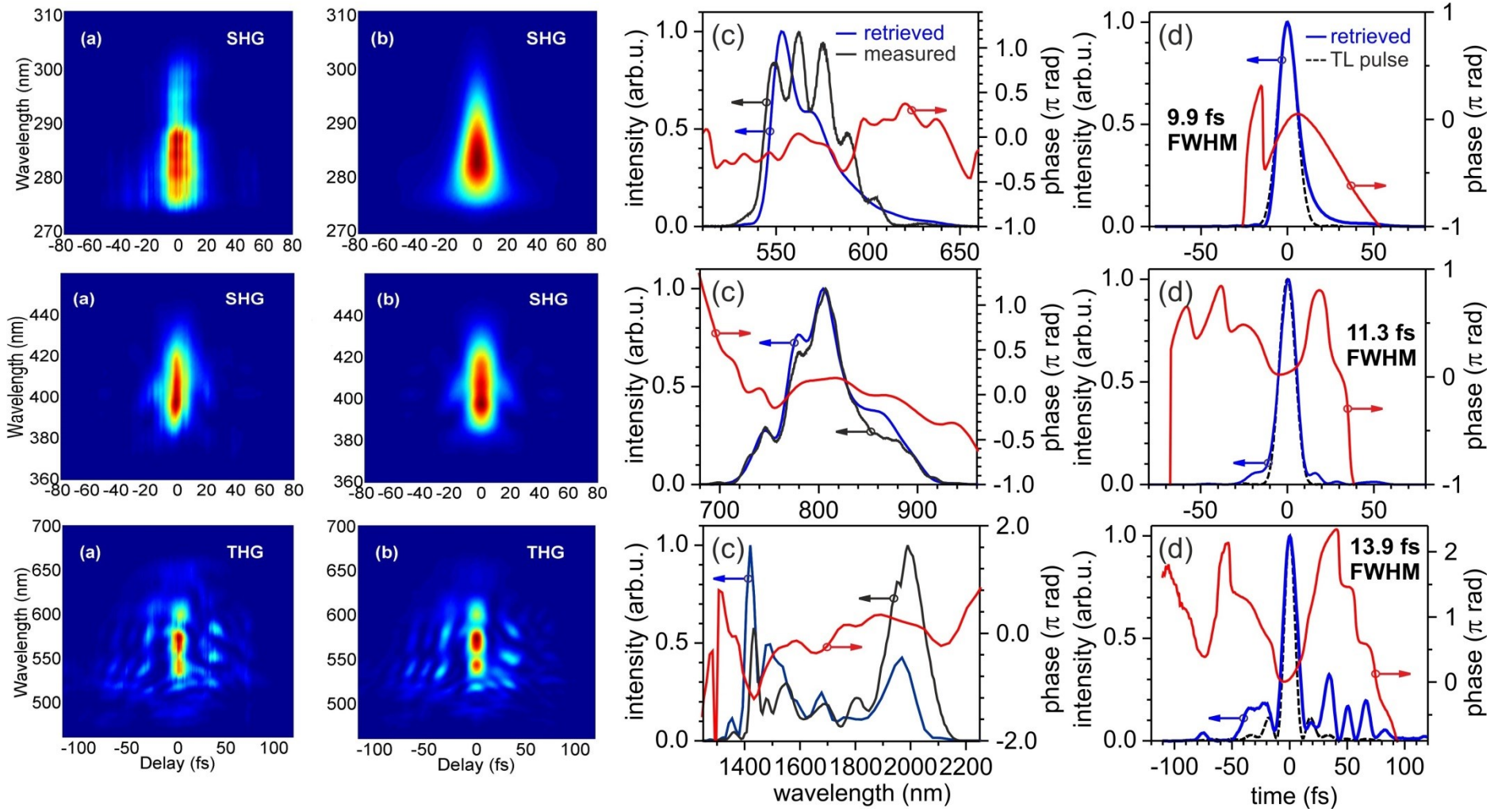


- recompressed all channels simultaneously close to TL at **synthesis point**
- flexible dispersion compensation scheme can be used at multi-mJ level

O. D. Mücke *et al.*, IEEE J. Sel. Top. Quantum Electron. **21**, 8700712 (2015)

# Parametric sub-cycle optical waveform synthesizers

3 possible synthesized $E(t)$, computed form the FROG-retrieved pulses (2nd stage)

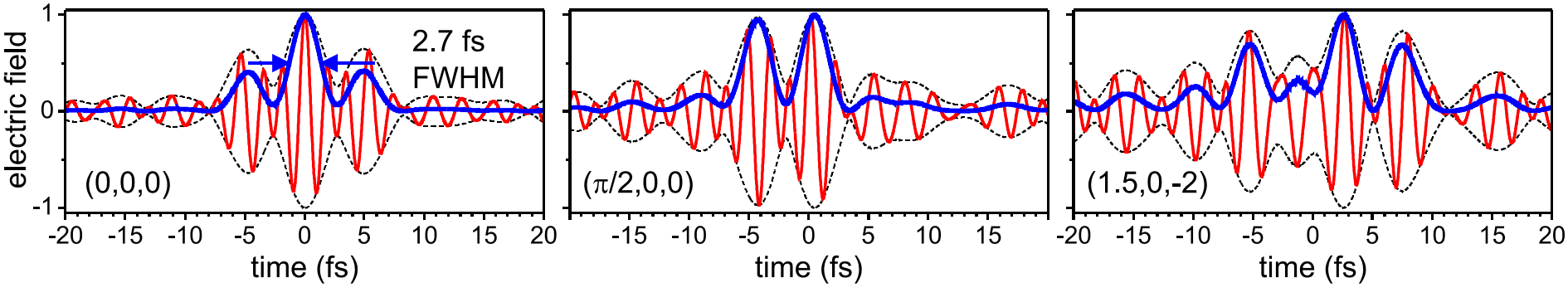


**Ongoing: recompress more broadband spectra → TL 1.9 fs**

**complete locking of relative timing and phase**

O. D. Mücke *et al.*, IEEE J. Sel. Top. Quantum Electron. **21**, 8700712 (2015)